J. Micropalaeontology, 42, 147–169, 2023
https://doi.org/10.5194/jm-42-147-2023

Journal of Micropalaeontology
Open Access

Bio-sequence stratigraphy of the Neogene: an example from El-Wastani gas field, onshore Nile Delta, Egypt

Ramadan M. El-Kahawy, Nabil Aboul-Ela, Ahmed N. El-Barkooky, and Walid G. Kassab

Geology Department, Faculty of Science, Cairo University, Cairo, Egypt

Correspondence: Ramadan M. El-Kahawy (relkahawy@sci.cu.edu.eg) and Walid G. Kassab (wkassab@cu.edu.eg)

Received: 11 October 2022 – Revised: 13 July 2023 – Accepted: 5 August 2023 – Published: 4 October 2023

Abstract. Due to modern hydrocarbon development and exploration activities throughout the onshore Nile Delta of Egypt, a high-resolution biochronologic sequence stratigraphy of the Neogene sequence was conducted to illustrate the gas-bearing reservoirs' depositional sequences. Our study used a multidisciplinary approach comprising biostratigraphy, facies analysis, geophysical logs, and seismic data to shed light on the Neogene stratigraphic framework. The biostratigraphic analysis of planktonic foraminifera and calcareous nannofossils allowed the recognition of six zones and/or subzones and nine zones, respectively. An open-shelf environment was suggested for the Middle–Upper Miocene Sidi Salem Formation, while the Upper Miocene Qawasim and Abu Madi formations were deposited under stressed environmental conditions interpreted as estuary facies. The Lower Pliocene (Zanclean) succession deposited in the middle to outer shelf domains, including the upper-bathyal environments. Seven depositional sequences bounded by six major sequence boundaries were recognized from Serravallian to Zanclean times. These boundaries significantly influenced changes in reservoir properties and architecture of the incised valley fills. The sea-level oscillations are interpreted by correlating the sequence boundaries and flooding surfaces with global eustatic charts.

1 Introduction

The architecture of the Nile Delta system is critical to understand the eastern Mediterranean plate tectonics. It is located along the northern margin of the African Plate, which extends from the Tethys subduction zones to the rift of the Red Sea, which separates it from the Arabian Plate. The geological study of the Nile Delta was initiated in the early 1960s, when oil corporations began drilling in the area. Due to modern exploration and use of geological and geophysical modelling approaches, this province provided some hidden hydrocarbon resources (EGPC, 1994). The Nile Delta is characterized by a thick sequence of Neogene clastic deposits, which represent one of the most significant gas provinces in Egypt (El-Heiny et al., 1990; Abdel al et al., 2000; El-Barkooky and Helal, 2002; Ismail et al., 2010; El-Kahawy et al., 2022; Selim et al., 2022). The Messinian onshore Nile Delta reservoirs were sedimentologically assessed, and their significant potential as reservoirs was confirmed (Selim et al., 2021).

The delta architecture is characterized by several palaeo-highs and palaeo-lows, thereby influencing facies distribution of the Nile Delta. Correlation of the different sub-basins using biostratigraphy is a powerful tool in establishing the sequence stratigraphy framework of the Nile Delta. Our aim is to clarify the Nile Delta stratigraphic framework using well-constrained biostratigraphic data integrated with 2D seismic profiles, wireline logs, and sequence stratigraphic analysis. We also introduced a quantitative analysis of foraminifera and calcareous nannofossils to investigate their relationships to system tracts compared to gamma rays and CycloLog patterns.

2 Geologic background and lithostratigraphy

The Nile Delta (Fig. 1a) is considered a significant hydrocarbon reservoir in the south-eastern Mediterranean region. The Nile Delta is composed of two significant provinces (Sestini, 1995), a deep offshore and an onshore sector. The deep

offshore domain received substantial sediment input (3500 m in 4–5 Myr) during the Plio-Pleistocene. It was affected by extensive Pliocene listric faults; prominent rollovers; rotated blocks; and slumping, particularly oriented toward the north-north-east and north-east. The onshore sector was dissected into northern and southern sub-basins to the south and to the north by a flexure zone termed the hinge line. The geometry of the pre-Miocene strata is influenced by the east–west-trending hinge line, through the mid-delta area (Said, 1981).

The southern-delta province (10 600 km^2) displays northward-dipping middle Eocene carbonates, indicated by asymmetric folds associated with the Syrian arc system that extends to the southern part of the Nile Delta and the Western Desert (Kamel et al., 1998). Deep pre-Tortonian faults with an east–west trend are most probably related to Eocene or Late Cretaceous tectonic events. Another fault system corresponds to post-Messinian deformations, mostly due to sediment loading along an unstable Nile Delta margin. These are normal faults also related to slumping and diapir rises in uncompacted Pliocene sediments and Messinian evaporites (Kamel et al., 1998).

From the Neogene to the Quaternary, the geological history of the Nile Delta has been subdivided into three cycles: Miocene, Plio-Pleistocene, and Holocene in age (Rizzini et al., 1978). The base of the Miocene cycle is represented by the Sidi Salem Formation, which is overlain by the Messinian Qawasim, Abu Madi, and Rosetta formations with fluvio-marine facies (Fig. 1d). The second cycle is characterized by clay deposits of Plio-Pleistocene age, with the Kafr El-Sheikh, El-Wastani, and Mit Ghamr formations (Fig. 1d). The third cycle consists of the Holocene Bilqas Formation composed of clays and subordinate sandstone beds. The Sidi Salem, Qawasim, Abu Madi, and Kafr El-Sheikh rock units (from older to younger) have been investigated (Fig. 1d).

3 Materials and methods

A collection of 151 subsurface ditch cutting samples was obtained from five wells located in the El-Wastani field (Fig. 1a, b, and c), spanning the Neogene successions of the Nile Delta.

The foraminiferal content was studied in 20 g of drilled cutting samples. A hydrogen peroxide solution (15 %) was used to soak the crushed samples in water. The solution was then sieved with a 63 µm mesh to filter the finest fractions. The residue was dried at low temperature (60 °C) and screened through a series of sieves (63, 125, 250, and 400 µm). The foraminifera species have been analysed using a Leica stereo-binocular microscope of the sieve-filtered fractions > 63 µm. The identification process is based on the schemes of Bolli and Saunders (1985) and Loeblich and Tappan (1988). The full taxonomic list of the planktonic and benthic foraminiferal taxa is provided in Appendix A.

To study calcareous nannofossils, samples have been prepared according to the method of Fornaciari et al. (1996). To capture the scarcer calcareous nannofossil taxa, each sediment sample was subjected to three replicates, from the bottom, middle, and top of the water column in the beaker. During microscopy, six traverses were examined; each traverse consisting of over 500 fields of view (FOVs) has been screened, and all the encountered specimens were counted after a quick slide analysis to detect the rare taxa. Relative abundance is estimated as follows: > 40 specimens in 500 FOVs is considered abundant, 30–40 is considered common, 20–30 is considered frequent, 10–20 is considered rare, and < 10 specimens is considered very rare (see File S2 in the Supplement). The taxonomic list of calcareous nannofossil taxa is presented in Appendix A.

The zonation schemes for planktonic foraminifera and calcareous nannofossils used in this study are based on Lirer et al. (2019), Agnini et al. (2017), Backman et al. (2012), Fornaciari et al. (1996), and Raffi et al. (2003), as established for the Mediterranean region. These schemes are correlated with the standard-zonation nannofossil schemes of Martini (1971) and Okada and Bukry (1980).

The scanning electron microscope (SEM) was used to capture the foraminiferal species, while we used a phase-contrast, light-polarized Nikon microscope at ×1000 magnification using a Tucsen digital camera to image calcareous nannofossil species.

The foraminiferal and calcareous nannofossil samples analysed in this study are curated at the Paleontological Museum of the Geology Department at Cairo University.

In this study, the gamma-ray log was analysed using the CycloLog software, as outlined by Nio et al. (2005). This software examines the frequency patterns of geophysical logs that are associated with facies, providing cyclic and stratigraphic approaches. By applying the CycloLog software to the gamma-ray log, two curves are generated: PEFA (prediction error filter analysis) and INPEFA (integrated prediction error filter analysis).

4 Results and discussion

4.1 Planktonic foraminiferal biostratigraphy

Six foraminiferal zones and/or subzones spanning the Middle Miocene to Lower Pliocene sequence have been identified based upon the recognition of 54 species and 34 genera of both planktonic (Figs. 2–3) and benthic (Figs. 4–5) foraminifera. We followed the biozonal scheme for planktonic foraminifera proposed by Lourens et al. (2004), Iaccarino (2007), and Lirer et al. (2019). The Mediterranean biozones were compared with other similar zones in geographically adjacent areas (Fig. 6). The similarities and dissimilarities between different authors are also discussed. The stratigraphic ranges of the recognized species (planktonic

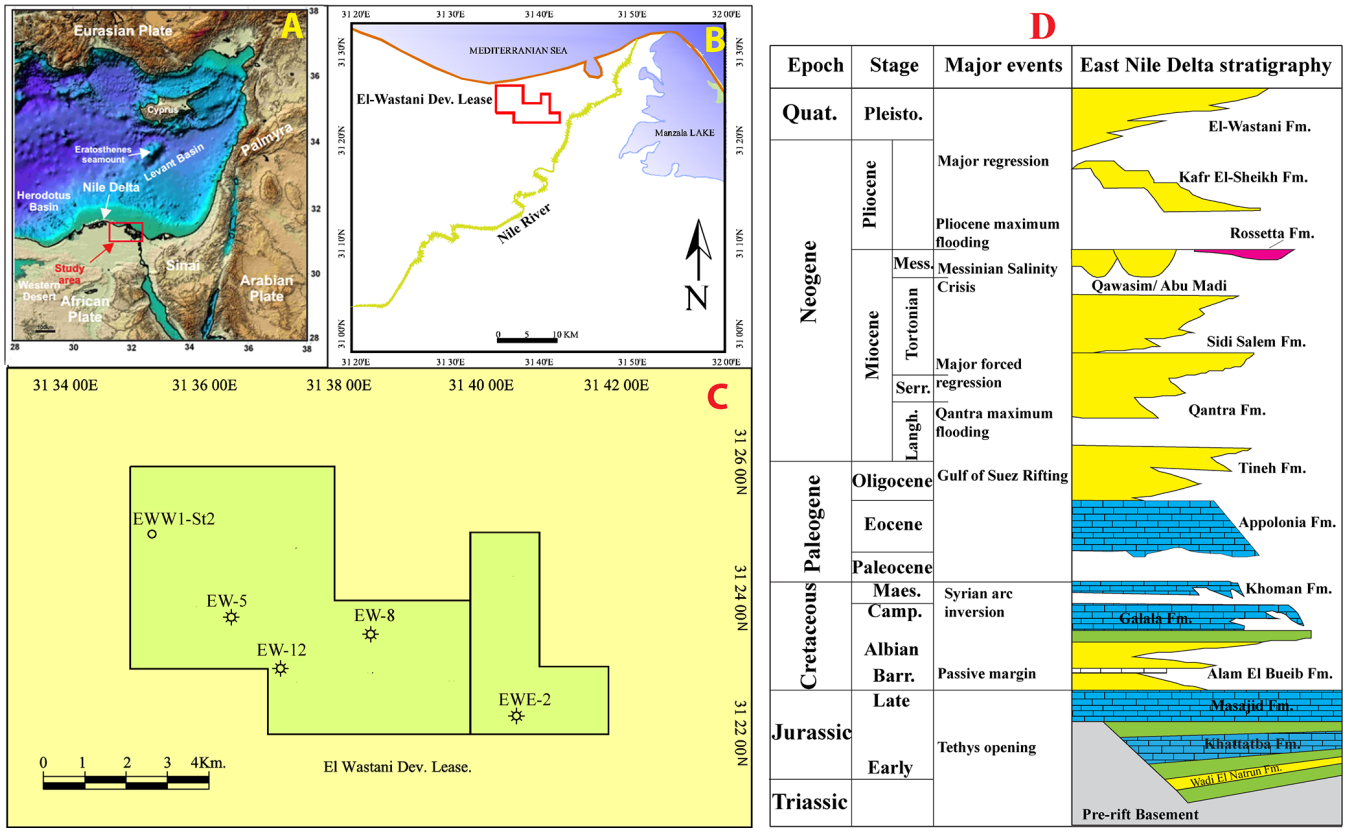

Figure 1. **(a)** Location map of the study area (Kellner et al., 2018), **(b)** map showing El-Wastani development lease concession, **(c)** zoomed map highlighting the studied wells, and **(d)** Nile Delta tectono-stratigraphic column (modified after Dolson et al., 2005).

and benthic) in the investigated wells are quantitatively presented in File 1 in the Supplement.

From bottom to top, the planktonic foraminiferal zones recorded in the studied wells are as follows.

4.1.1 *Paragloborotalia mayeri* total range subzone (MMi7b)

Definition. Sprovieri et al. (2002) designated this subzone as a biostratigraphic total range subzone between the lowest occurrence (LO) and highest occurrence (HO) of *Paragloborotalia mayeri*.

Occurrence. This subzone is 60 m thick and is only encountered in well EWE-2 at depths ranging from 3050 to 2950 m (Fig. 7e; see File 3 in the Supplement).

Assemblage. This planktonic foraminifer subzone comprises a rich and diversified benthic assemblage (File 1 in the Supplement).

Remarks. This zone corresponds to the Serravallian. In the Atlantic, it correlates with zone N12 of Blow (1969) and with the upper parts of N12 of Srinivasan and Kennett (1983) and Berggren et al. (1995). It is equivalent to M9b of Wade et al. (2011), based on the occurrence of *Paragloborotalia siakensis*. In the Nile Delta Basin, it corresponds to the *Globorotalia mayeri* zone of Abdou et al. (1984) and to the *Globorotalia fohsi* zone of Rizzini et al. (1976).

Age. Middle Miocene (Serravallian).

4.1.2 *Neogloboquadrina acostaensis* interval zone (MMi11)

Definition. It is defined as the interval between the LO of *Neogloboquadrina acostaensis* and the LO of the *Globigerinoides extremus*.

Occurrence. The biozone has only been encountered in wells EWW1-St2 and EW-5. It occurs at depths from 3300 to 3200 m in well EWW1-St2 and from 3300 to 3100 m in well EW-5, reaching a thickness of 100 and 200 m, respectively (Fig. 7e, d).

Assemblage. See File 1 in the Supplement.

Remarks. This biozone is congruent with zone N16 of Blow (1969). In the tropical environments, it is consistent with the *Neogloboquadrina acostaensis* (M13a) zone as suggested by Berggren et al. (1995) and Wade et al. (2011). It is correlated with the Mediterranean zone MMi11, as adopted by Lourens et al. (2004), Iaccarino et al. (2007), and Lirer et al. (2019). In the Nile Delta Basin, it is likely correlated with

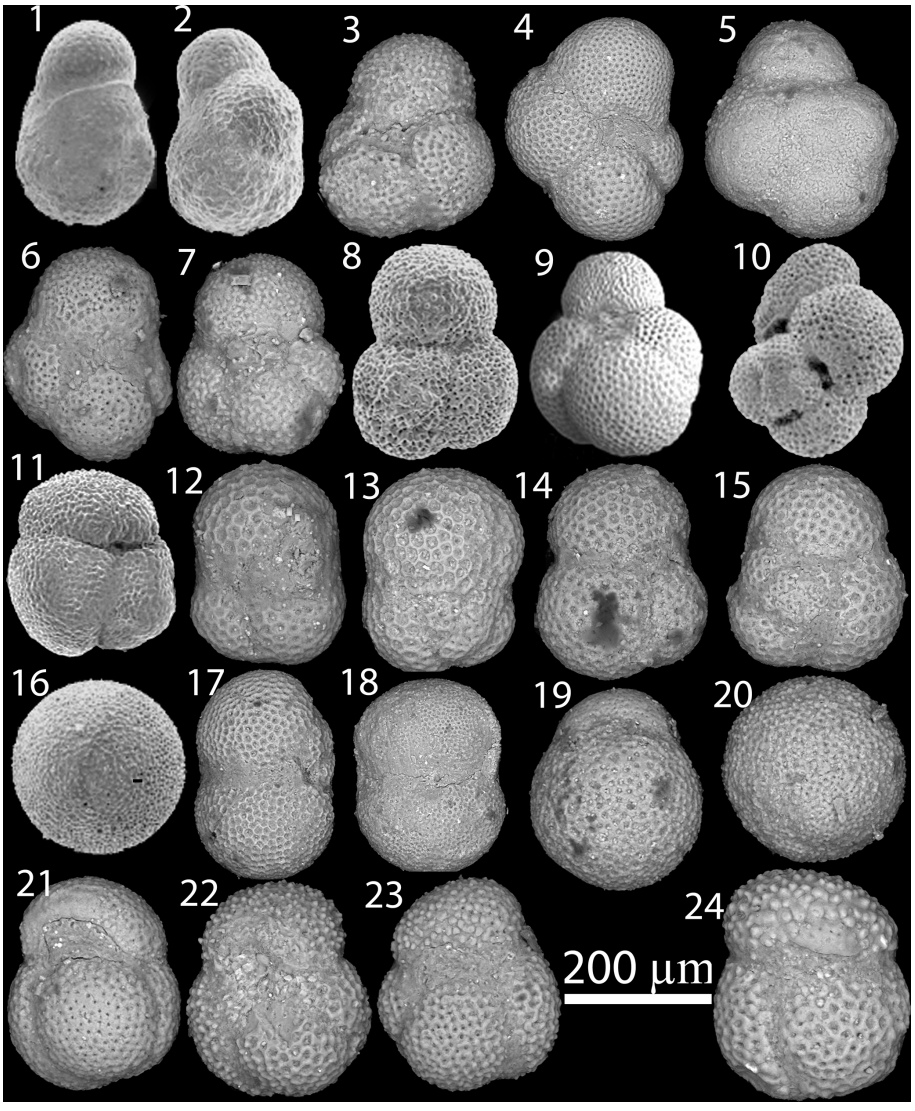

Figure 2. **(1–2)** *Globoturborotalita nepenthes*: **(1)** ventral view, **(2)** dorsal view; 2630 m depth, well EWE-2, Kafr El-Sheikh Fm. **(3–6)** *Globigerina bulloides*: **(3, 4, 6)** ventral view, **(5)** dorsal view; 2795 m depth, well EWW1-St2, Kafr El-Sheikh Fm. **(7–8)** *Globigerina falconensis*: **(7)** ventral view, **(8)** dorsal view; 3204 m depth, well EWW1-St2, Sidi Salem Fm. **(9–10)** *Trilobatus sacculifer*: **(9)** ventral view, **(10)** dorsal view; 2788 m depth, well EWW1-St2, Kafr El-Sheikh Fm. **(11)** *Globigerinoides conglobatus*: ventral view, 2721 m depth, well EW-12, Kafr El-Sheikh Fm. **(12–15)** *Trilobatus trilobus*: **(12, 13)** dorsal view, **(14, 15)** ventral view; 3204 m depth, well EWE-2, Sidi Salem Fm. **(16–18)** *Orbulina universa*: 2795 m depth, well EWW1-St2, Kafr El-Sheikh Fm. **(19–20)** *Orbulina suturalis*: 2615 m depth, well EWE-2, Kafr El-Sheikh Fm. **(21–24)** *Globigerinoides obliquus*: ventral views, 2615 m depth, well EWE-2, Kafr El-Sheikh Fm.

the upper part of the *Globorotalia menardii* zone (Rizzini et al., 1978).

Age. Late Miocene (Tortonian).

4.1.3 *Non-distinctive* interval zone (NDZ)

Definition. According to Iaccarino and Salvatorini (1982), this zone was originally defined as an interval determined by the transition in the coiling directions of *Neogloboquadrina acostaensis* from sinistral to dextral at its base and the first occurrence of *Globorotalia suterae* at the top. However, planktonic foraminifera lack this interval in our study. Subsequently, the zone is identified here based on a few sporadic occurrences of benthic foraminifera (*Ammonia beccarii* and *Elphidium* sp.) and ostracods (*Cyprideis* spp.).

Occurrence. The zone is recorded in wells EWE-2, EW-8, EW-12, EW-5, and EWW1-St2 at depths of 2950 to 2630 m, 3120 to 2670 m, 3105 to 2725 m, 3100 to 2650 m, and 3200 to 2805 m, respectively (Fig. 7a, b, c, d, and e). The respective thicknesses in the five wells are thus 320, 450, 380, 450, and 395 m.

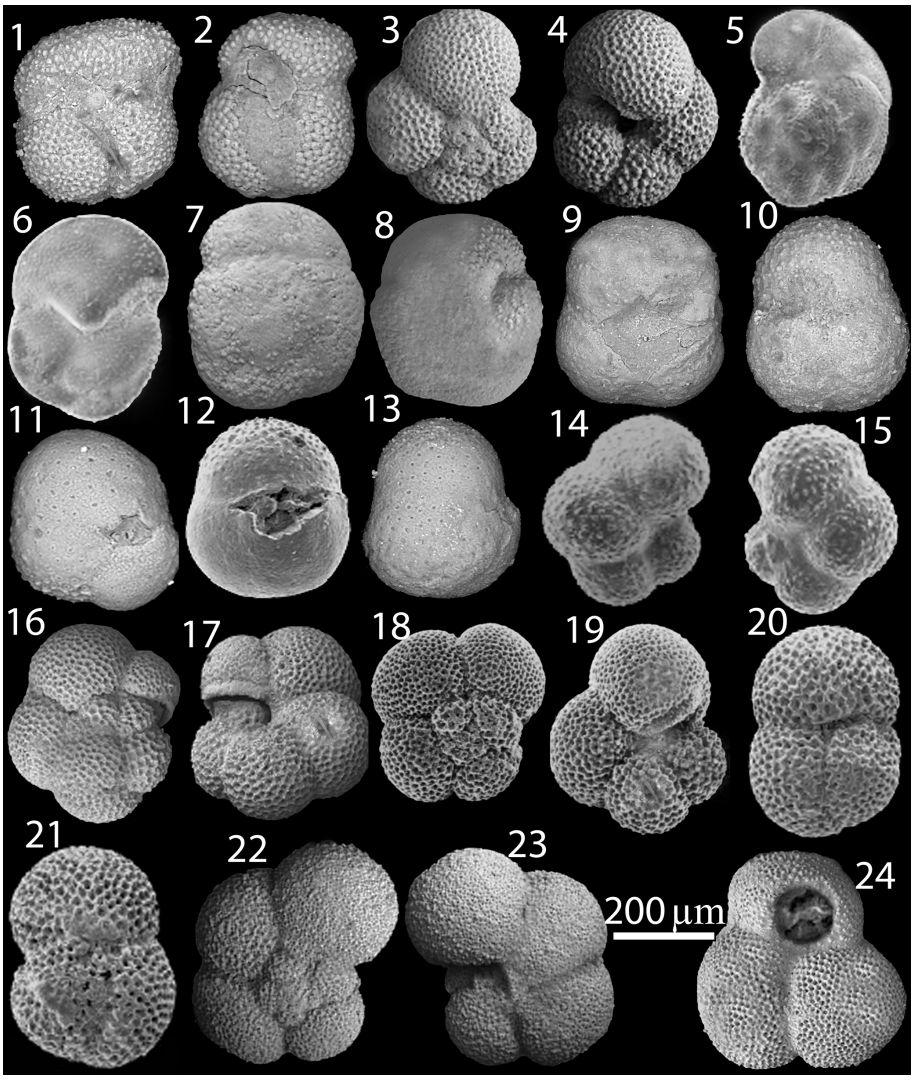

Figure 3. **(1–2)** *Globigerinoides extremus*: ventral views, 2665 m depth, well EW-8, Kafr El-Sheikh Fm. **(3–4)** *Paragloborotalia mayeri*: **(3)** dorsal view, **(4)** ventral view; 2990 m depth, well EWE-2, Sidi Salem Fm. **(5–6)** *Globorotalia margaritae*: **(5)** dorsal view, **(6)** ventral view; 2788 m depth, well EWW1-St2, Kafr El-Sheikh Fm. **(7–8)** *Globoconella puncticulata*: **(7)** dorsal view, **(8)** ventral view; 2760 m depth, well EWW1-St2, Kafr El-Sheikh Fm. **(9–10)** *Sphaeroidinellopsis seminulina*: ventral views, 2721 m depth, well EW-12, Kafr El-Sheikh Fm. **(11–13)** *Sphaeroidinellopsis paenedehiscens*: ventral views, 2795 m depth, well EWW1-St2, Kafr El-Sheikh Fm. **(14–15)** *Globigerinella siphonifera*: **(14)** ventral view, **(15)** dorsal view; 2555 m depth, well EW-5, Kafr El-Sheikh Fm. **(16–17)** *Neogloboquadrina acostaensis*: **(16)** dorsal view, **(17)** ventral view; 3300 m depth, well EWW1-St2, Sidi Salem Fm. **(18–19)** *Paragloborotalia continuosa*: **(18)** dorsal view, **(19)** ventral view; 2990 m depth, well EWE-2, Sidi Salem Fm. **(20–21)** *Trilobatus immaturus*: **(20)** ventral view, **(21)** dorsal view; 2650 m depth, well EW-5, Kafr El-Sheikh Fm. **(22–23)** *Globigerinella obesa*: **(22)** dorsal view, **(23)** ventral view; 3020 m depth, well EWE-2, Sidi Salem Fm. **(24)** *Globigerinoides ruber*: 2470 m depth, well EW-5, Kafr El-Sheikh Fm.

Remarks. This zone corresponds to zone N17 of Blow (1969). In the Mediterranean region, the NDZ is characteristic of the Messinian stage, as described by Iaccarino and Salvatorini (1982). Many works dealing with the eastern Mediterranean (i.e. Iaccarino et al., 2007; Lirer et al., 2019) have shown the absence of planktonic foraminifers in the NDZs. In the Atlantic domain, Berggren et al. (1995) recognized the Late Messinian age by the occurrence of *Globigerinoides extremus* (M14) and the lowermost part of the *Gt. tumida*/*Gt. nepenthes* (PL1), according to Wade et al. (2011). The non-distinctive interval zone characterizes the Late Miocene Messinian stage in the Nile Delta Basin (Rizzini et al., 1976; Farouk et al., 2014).

Age. Late Miocene (Messinian).

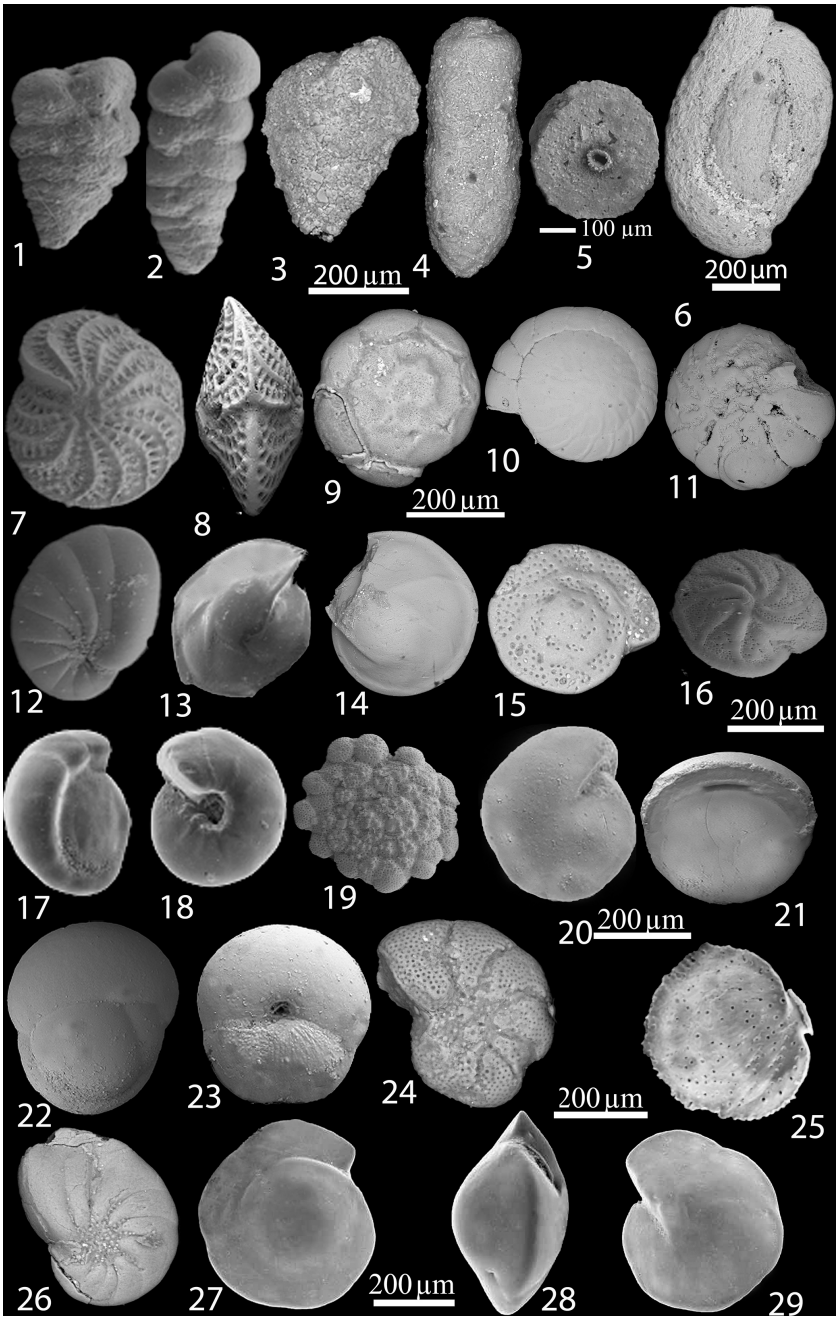

Figure 4. **(1)** *Textularia pseudorugosa*: 2565 m depth, well EWE-2, Kafr El-Sheikh Fm. **(2)** *Textularia* sp. 1: 2600 m depth, well EWE-2, Kafr El-Sheikh Fm. **(3)** *Textularia* sp. 2: 3050 m depth, well EWE-2, Sidi Salem Fm. **(4–5)** *Martinottiella communis*: 2600 m depth, well EWE-2, Kafr El-Sheikh Fm. **(6)** *Quinqueloculina* sp.: 2585 m depth, well EW-8, Kafr El-Sheikh Fm. **(7–8)** *Elphidium* sp.: **(7)** dorsal view, **(8)** side view; 2945 m depth, well EWE-2, Qawasim Fm. **(9–11)** *Ammonia beccarii*: **(9–10)** dorsal view, **(11)** ventral view; 2700 m depth, well EW-8, Abu Madi Fm. **(12)** *Nonionoides turgidus*: 2600 m depth, well EWE-2, Kafr El-Sheikh Fm. **(13)** *Lenticulina calcar*: 3280 m depth, well EWW1-St2, Sidi Salem Fm. **(14)** *Lenticulina inornata*: 3050 m depth, well EWE-2, Sidi Salem Fm. **(15–16)** *Heterolepa praecincta*: **(15)** dorsal view, **(16)** ventral view; 3020 m depth, well EWE-2, Sidi Salem Fm. **(17–18)** *Hansenisca soldanii*: **(17)** ventral view, **(18)** dorsal view; 2565 m depth, well EWE-2, Kafr El-Sheikh Fm. **(19)** *Planorbulina mediterranensis*: 2565 m depth, well EWE-2, Kafr El-Sheikh Fm. **(20–21)** *Pullenia bulloides*: **(20)** side view, **(21)** apertural view; 2615 m depth, well EWE-2, Kafr El-Sheikh Fm. **(22–23)** *Sphaeroidina bulloides*: **(22)** dorsal view, **(23)** ventral view; 2580 m depth, well EW-5, Kafr El-Sheikh Fm. **(24)** *Epistomaroides* sp.: 2780 m depth, well EWW1-St2, Kafr El-Sheikh Fm. **(25)** *Siphonina reticulata*: 2550 m depth, well EW-12, Kafr El-Sheikh Fm. **(26)** *Nonionella chiliensis*: 2580 m depth, well EWE-2, Kafr El-Sheikh Fm. **(27–29)** *Oridorsalis umbonatus*: **(27)** dorsal view, **(28)** side view, **(29)** ventral view; 2805 m depth, well EWW1-St2, Kafr El-Sheikh Fm.

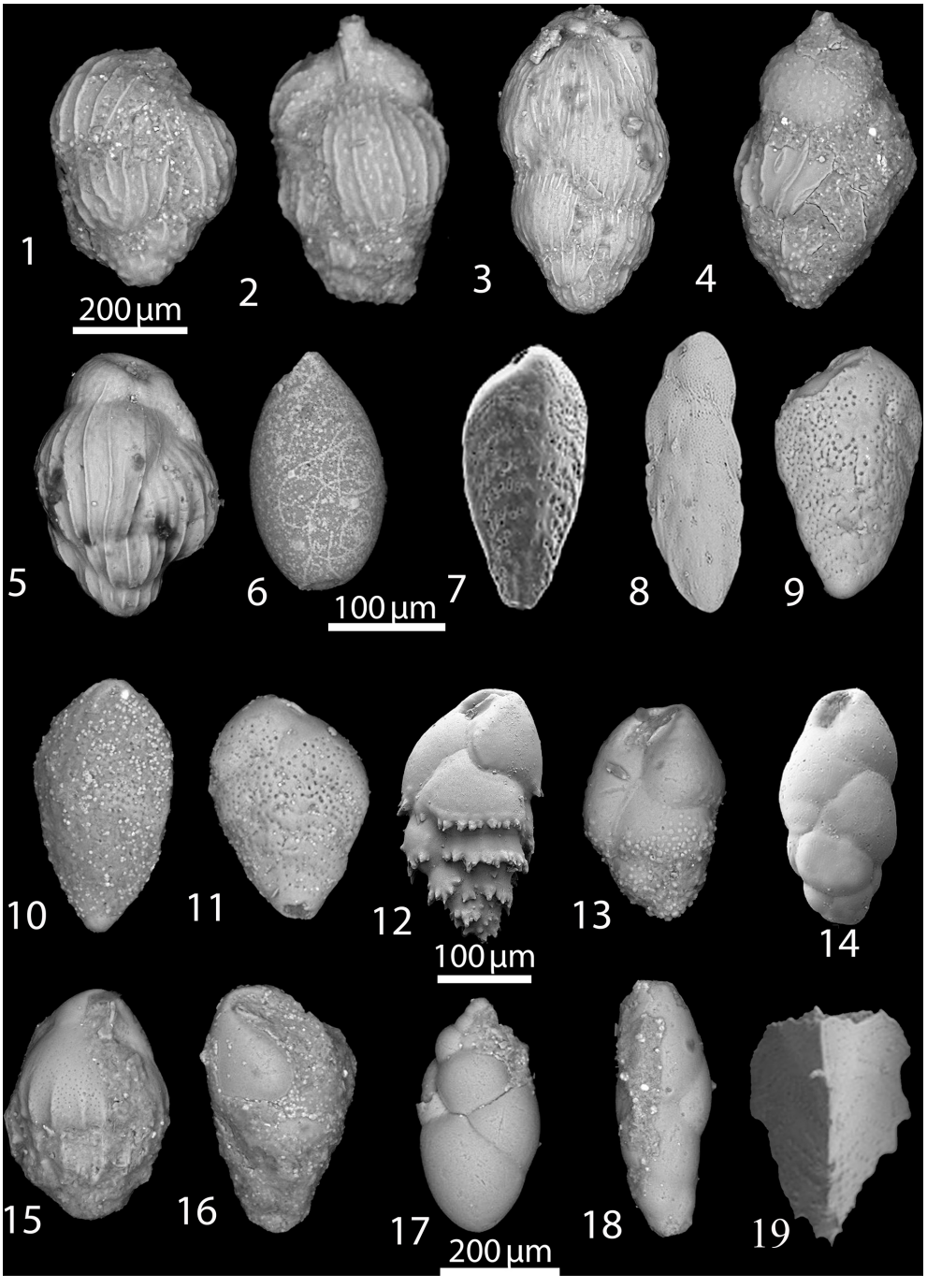

Figure 5. **(1–2)** *Uvigerina peregrina*: 2780 m depth, well EWW1-St2, Kafr El-Sheikh Fm. **(3)** *Uvigerina semiornata*: 3040 m depth, well EWE-2, Sidi Salem Fm. **(4)** *Rectuvigerina* sp.: 2600 m depth, well EWE-2, Kafr El-Sheikh Fm. **(5)** *Uvigerina striatissima*: 2990 m depth, well EWE-2, Sidi Salem Fm. **(6)** *Oolina laevigata*: 2580 m depth, well EWE-2, Kafr El-Sheikh Fm. **(7)** *Bolivina dilatata*: 2600 m depth, well EW-8, Kafr El-Sheikh Fm. **(8)** *Brizalina striatula*: 2670 m depth, well EW-8, Kafr El-Sheikh Fm. **(9–10)** *Bolivina spathulata*: 2615 m depth, well EW-5, Kafr El-Sheikh Fm. **(11)** *Brizalina* sp.: 2610 m depth, well EW-8, Kafr El-Sheikh Fm. **(12–13)** *Bulimina marginata*: 2580 m depth, well EWE-2, Kafr El-Sheikh Fm. **(14)** *Bulimina elongata*: 2780 m depth, well EWW1-St2, Kafr El-Sheikh Fm. **(15)** *Bulimina striata*: 2470 m depth, well EW-5, Kafr El-Sheikh Fm. **(16)** *Protoglobobulimina pupoides*: 2780 m depth, well EWW1-St2, Kafr El-Sheikh Fm. **(17)** *Fursenkoina seminuda*: 2760 m depth, well EWW1-St2, Kafr El-Sheikh Fm. **(18)** *Fursenkoina* sp.: 2725 m depth, well EW-12, Kafr El-Sheikh Fm. **(19)** *Reussella spinulosa*: 2600 m depth, well EWE-2, Kafr El-Sheikh Fm.

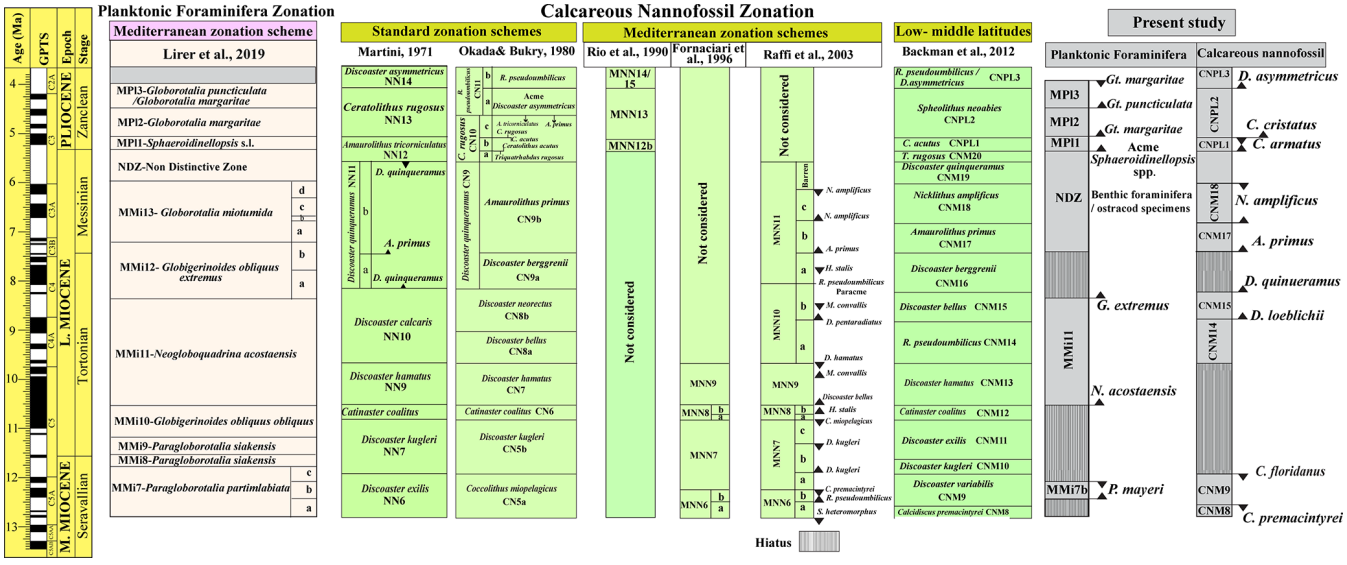

Figure 6. Biostratigraphic correlation chart of the proposed Middle Miocene–Early Pliocene biozones with other biozones in the Mediterranean realm.

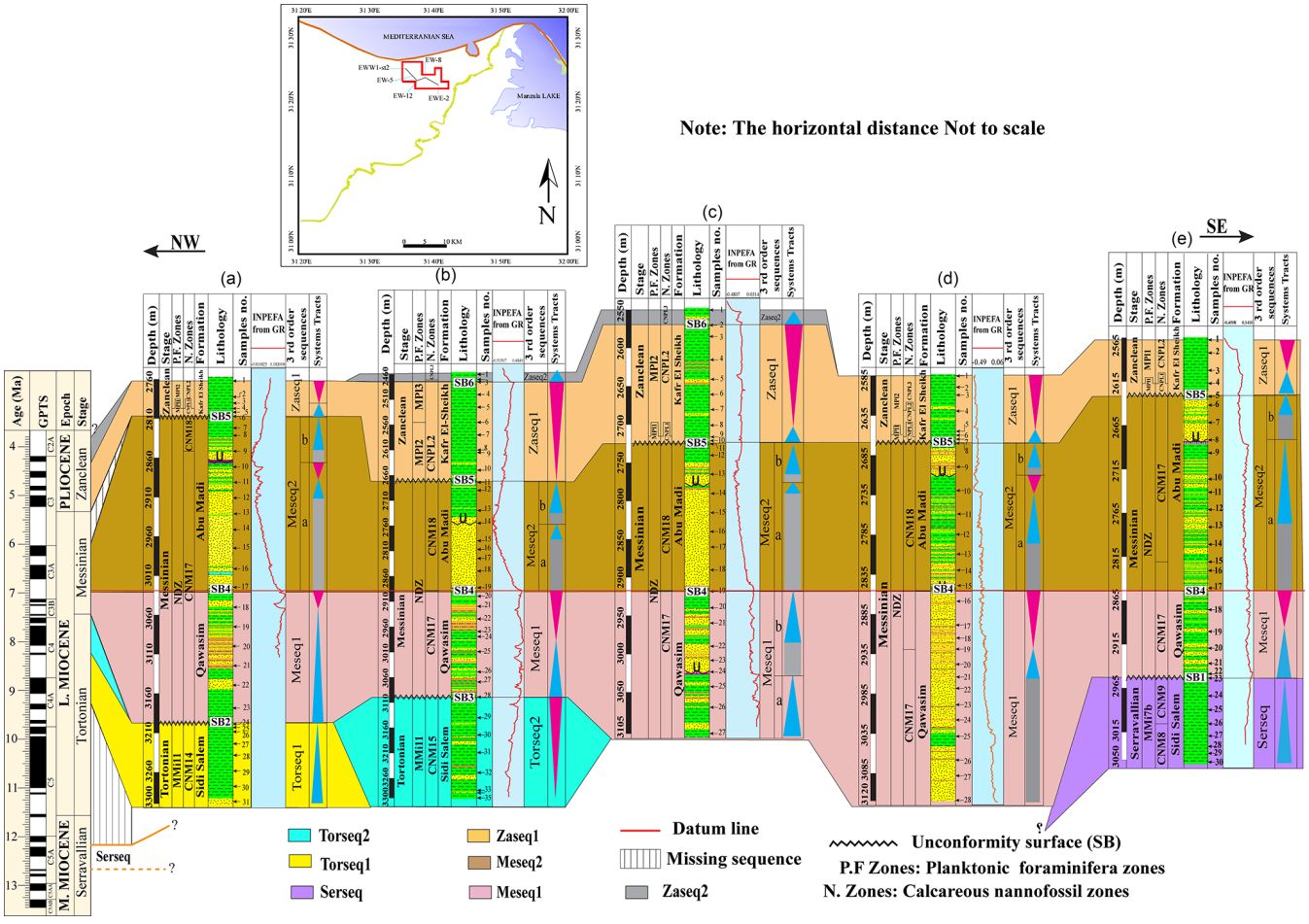

Figure 7. Time-based depositional sequence correlation of the Middle Miocene–Early Pliocene along the NW–SE direction of El-Wastani field. **(a)** EWE-2, **(b)** EW-8, **(c)** EW-12, **(d)** EW-5, and **(e)** EWW1-St2.

4.1.4 *Sphaeroidinellopsis seminulina* interval zone (MPl1)

Definition. This interval zone comprises the LO of *Sphaeroidinellopsis* spp., as a common occurrence, and the LO of *Globorotalia margaritae*.

Occurrence. The zone has been encountered in the basal part of the Kafr El-Sheikh Formation from wells EWE-2, EW-8, EW-12, and EWW1-St2. The monitored depths in the four wells are from 2805 to 2788 m, 2670 to 2660 m, 2725 to 2717 m, and 2630 to 2615 m, respectively (Fig. 7a–c and e). Therefore, the thickness of this zone varies as follows: 17, 15, 8, and 15 m.

Assemblage. See File 1 in the Supplement.

Remarks. Following Cita (1975), Iaccarino and Salvatorini (1982), and Iaccarino (1985), the occurrence of *Sphaeroidinellopsis seminulina* in the Mediterranean corresponds to zone N18 of Blow (1969) of Early Pliocene age. This zone also corresponds to the Mediterranean zone MPl1, where the top horizon has been placed according to the first frequent occurrence of *Globorotalia margaritae* (Lourens et al., 2004; Iaccarino et al., 2007; Lirer et al., 2019). This biozone also corresponds to the lower part of the *Globorotalia tumida/Globoturborotalita nepenthes* (PL1) in the Atlantic and Pacific oceans (Wade et al., 2011). The same zone was recorded in the Early Pliocene by Rizzini (1978) and Abdou et al. (1984) in the Nile Delta. Conversely, Ismail et al. (2010) determined the Early Pliocene with the *Globorotalia margaritae* zone.

Age. Early Pliocene (Zanclean).

4.1.5 *Globorotalia margaritae* interval zone (MPl2)

Definition. This zone was drawn from the LO of *Globorotalia margaritae* to the LO of *Globorotalia puncticulata*.

Occurrence. This biozone has been recorded in the Kafr El-Sheikh Formation of all investigated wells (EWE-2, EW-8, EW-12, EW-5, and EWW1-St2) (Fig. 7a–e). The zone encompasses the following depth intervals in the five cited wells: 2615 to 2565 m, 2660 to 2585 m, 2717 to 2550 m, 2650 to 2555 m, and 2788 to 2760 m, with thicknesses of 28, 75, 167, 95, and 50 m, respectively (Fig. 7a–e).

Assemblage. A quite rich and distinctive planktonic and benthic foraminiferal assemblage has been recorded. See File 1 in the Supplement.

Remarks. According to Blow (1969), this zone coincides with the lower part of his zone N19. It is comparable to the *Globorotalia margaritae* zone, which is found in the Mediterranean area (Borsetti et al., 1979; Iaccarino and Salvatorini, 1982). According to Lirer et al. (2019) and Lourens et al. (2004), it corresponds to zone MPl2 of Zanclean age (Early Pliocene). In the Nile Delta Basin, the recognized zone belongs to the *Globorotalia margaritae* zone (Rizzini et al., 1976; Abdel-Kireem et al., 1984), whereas it corresponds to the lowermost part of the *Globorotalia puncticulata* zone of Abdou et al. (1984).

Age. Early Pliocene (Zanclean).

4.1.6 *Globorotalia puncticulata/Globorotalia margaritae* concurrent range zone (MPl3)

Definition. It is defined as the interval characterized by the concomitant presence of *Globorotalia puncticulata* (after its LO) and *Globorotalia margaritae* (before its HO).

Occurrence. This zone has been recorded only in the Kafr El-Sheikh Formation of well EW-5 and spans the interval from 2555 to 2460 m (95 m thick; Fig. 7d). Due to the poor preservation state of the foraminifera specimens, this zone is not recorded in the other wells.

Assemblage. The benthic foraminifers recovered from this interval are highly diversified and abundant. See File 1 in the Supplement.

Remarks. It is suggested that the proposed biozone spans the upper zone N19, in accordance with Blow (1969). In the Mediterranean realm, the recognized zone is consistent with zone MPl3 of Lirer et al. (2019) and others. It also matches with the lower part of the *Globorotalia puncticulata* zone in the eastern Mediterranean region (Borsetti et al., 1979). The identified zone has been correlated in part with the *Globorotalia puncticulata* zone of Rizzini (1978), Abdel-Kireem et al. (1984), and El-Heiny et al. (1990) of the Nile Delta Basin and of the Red Sea (Selima, 1998).

Age. Early Pliocene (Zanclean).

4.1.7 Calcareous nannofossil biostratigraphy

The five studied Middle Miocene–Lower Pliocene successions show a diversified calcareous nannofossil assemblage (Figs. 8 and 9). The identification of 54 species, along with their stratigraphic distribution, allowed the definition of 9 calcareous nannofossil zones. Such zones are compared to those published for the Mediterranean realm (Fig. 6). The distribution of various calcareous nannofossil species, their equivalent zones/subzones, and proposed ages in the five wells are illustrated in File 2 in the Supplement.

The recorded calcareous nannofossil zones are from bottom to top.

4.1.8 *Calcidiscus premacintyrei* interval zone (CNM8)

Definition. This zone was defined as the interval from the HO of *Sphenolithus heteromorphus* to the HO of *Calcidiscus premacintyrei*.

Occurrence. This zone has been recorded only in well EWE-2, spanning depths from 3050 to 2990 m, where the Sidi Salem Formation has a thickness of ∼ 60 m (Fig. 7a).

Assemblage. See File 2 in the Supplement.

Remarks. Zone CNM8 (*Calcidiscus premacintyrei*) of Backman et al. (2012) coincides with the lower parts of zone

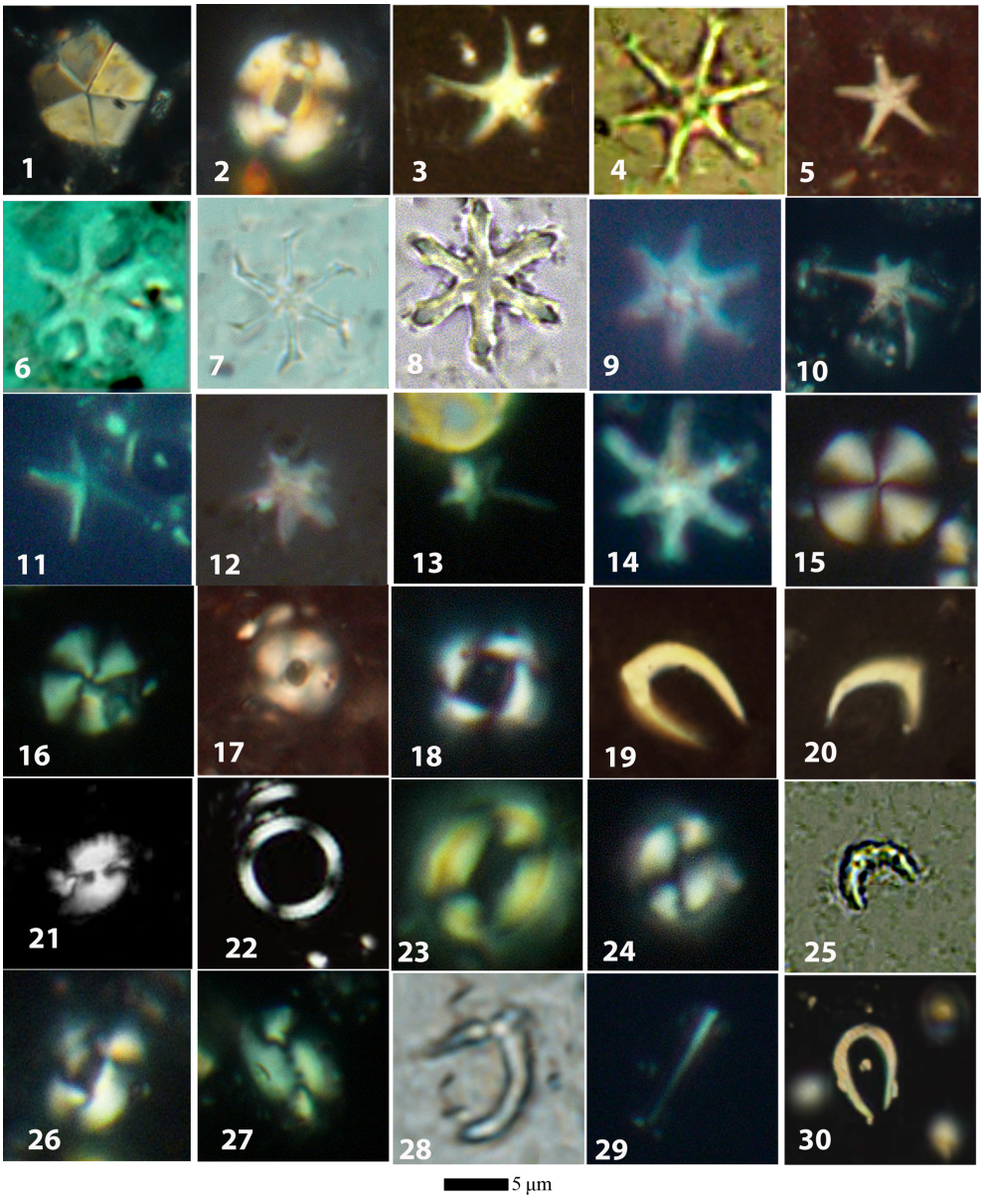

Figure 8. **(1)** *Braarudosphaera bigelowii*: 2795 m depth, well EWW1-St2, Kafr El-Sheikh Fm. **(2)** *Calcidiscus premacintyrei*: 2990 m depth, well EWE-2, Sidi Salem Fm. **(3)** *Discoaster quinqueramus*: 2805 m depth, well EWW1-St2, Kafr El-Sheikh Fm. **(4)** *Discoaster exilis*: 2990 m depth, well EWE-2, Sidi Salem Fm. **(5)** *Discoaster pentaradiatus*: 2788 m depth, well EWW1-St2, Kafr El-Sheikh Fm. **(6)** *Discoaster variabilis*: 2615 m depth, well EWE-2, Kafr El-Sheikh Fm. **(7)** *Discoaster loeblichii*: 3204 m depth, well EWW1-St2, Sidi Salem Fm. **(8)** *Discoaster surculus*: 2615 m depth, well EWE-2, Kafr El-Sheikh Fm. **(9)** *Discoaster bollii*: 3204 m depth, well EWW1-St2, Sidi Salem Fm. **(10)** *Discoaster brouweri*: 2615 m depth, well EWE-2, Kafr El-Sheikh Fm. **(11)** *Discoaster bellus*: 3240 m depth, well EWW1-St2, Sidi Salem Fm. **(12)** *Discoaster berggrenii*: 2875 m depth, well EWE-2, Qawasim Fm. **(13)** *Discoaster asymmetricus*: 2460 m depth, well EWW1-St2, Kafr El-Sheikh Fm. **(14)** *Discoaster* sp.: 2630 m depth, well EWE-2, Kafr El-Sheikh Fm. **(15–16)** *Calcidiscus leptoporus*: 2788 m depth, well EWW1-St2, Kafr El-Sheikh Fm. **(17)** *Calcidiscus macintyrei*: 2788 m depth, well EWW1-St2, Kafr El-Sheikh Fm. **(18)** *Reticulofenestra rotaria*: 2790 m depth, well EW-5, Abu Madi Fm. **(19)** *Ceratolithus cristatus*: 2565 m depth, well EWE-2, Kafr El-Sheikh Fm. **(20)** *Ceratolithus armatus*: 2795 m depth, well EWW1-St2, Kafr El-Sheikh Fm. **(21)** *Helicosphaera sellii*: 2795 m depth, well EWW1-St2, Kafr El-Sheikh Fm. **(22)** *Coronocyclus nitescens*: 3020 m depth, well EWE-2, Sidi Salem Fm. **(23)** *Coccolithus miopelagicus*: 2985 m depth, well EWE-2, Sidi Salem Fm. **(24)** *Coccolithus pelagicus*: 2630 m depth, well EWE-2, Kafr El-Sheikh Fm. **(25)** *Amaurolithus primus*: 2760 m depth, well EWW1-St2, Kafr El-Sheikh Fm. **(26)** *Cyclicargolithus floridanus*: 2990 m depth, well EWE-2, Sidi Salem Fm. **(27)** *Helicosphaera carteri*: 2665 m depth, well EW-8, Kafr El-Sheikh Fm. **(28)** *Amaurolithus tricorniculatus*: 2795 m depth, well EWW1-St2, Kafr El-Sheikh Fm. **(29)** *Rhabdosphaera clavigera*: 2760 m depth, well EWE-2, Abu Madi Fm. **(30)** *Amaurolithus delicatus*: 2795 m depth, well EWW1-St2, Kafr El-Sheikh Fm.

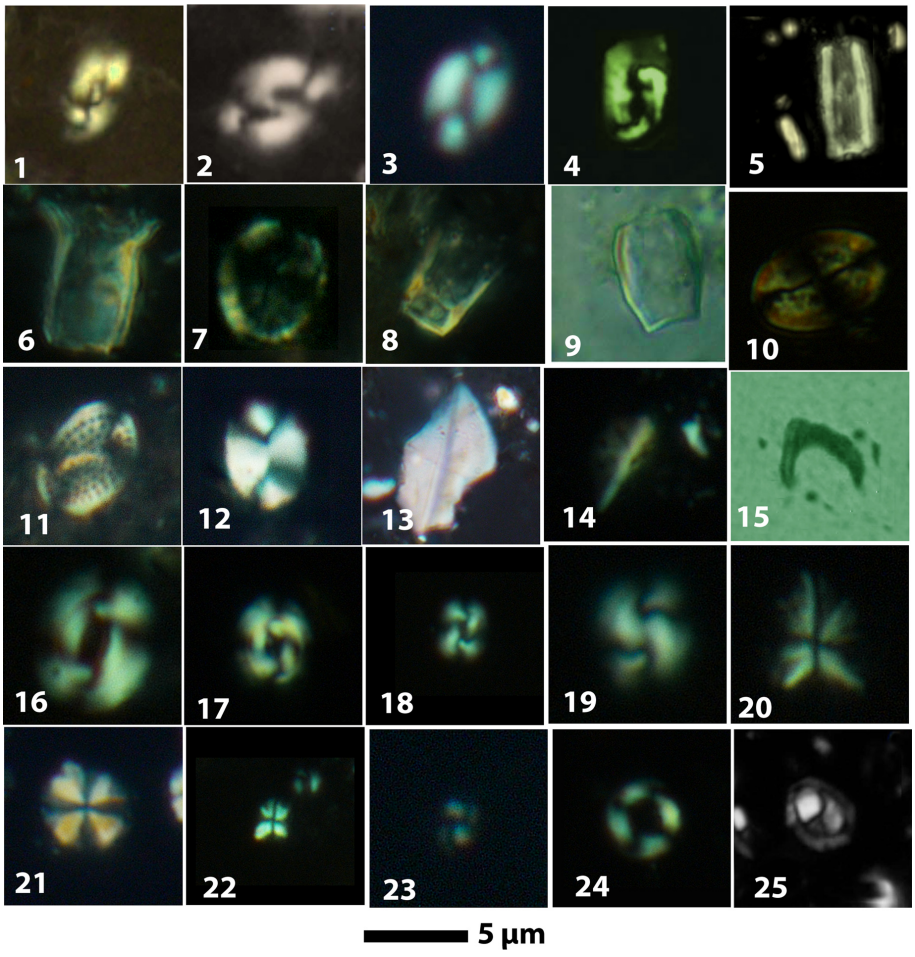

Figure 9. **(1)** *Helicosphaera intermedia*: 2630 m depth, well EWE-2, Kafr El-Sheikh Fm. **(2)** *Helicosphaera stalis*: 2950 m depth, well EWE-2, Qawasim Fm. **(3)** *Helicosphaera walbersdorfensis*: 3050 m depth, well EWE-2, Sidi Salem Fm. **(4)** *Helicosphaera orientalis*: 2830 m depth, well EWW1-St2, Abu Madi Fm. **(5)** *Scyphosphaera lagena*: 2788 m depth, well EWW1-St2, Kafr El-Sheikh Fm. **(6)** *Scyphosphaera pulcherrima*: 2565 m depth, well EWE-2, Kafr El-Sheikh Fm. **(7)** *Scyphosphaera globulata*: 2615 m depth, well EWE-2, Kafr El-Sheikh Fm. **(8)** *Scyphosphaera porosa*: 2615 m depth, well EWE-2, Kafr El-Sheikh Fm. **(9)** *Scyphosphaera apsteinii*: 2795 m depth, well EWW1-St2, Kafr El-Sheikh Fm. **(10)** *Pontosphaera discopora*: 2795 m depth, well EWW1-St2, Kafr El-Sheikh Fm. **(11)** *Pontosphaera multipora*: 3210 m depth, well EWE-2, Sidi Salem Fm. **(12)** *Pontosphaera japonica*: 2615 m depth, well EWE-2, Kafr El-Sheikh Fm. **(13)** *Orthorhabdus rugosus*: 2800 m depth, well EWE-2, Abu Madi Fm. **(14)** *Orthorhabdus serratus*: 3040 m depth, well EWE-2, Sidi Salem Fm. **(15)** *Nicklithus amplificus*: 2730 m depth, well EWE-2, Abu Madi Fm. **(16)** *Reticulofenestra pseudoumbilicus*: 2630 m depth, well EWE-2, Kafr El-Sheikh Fm. **(17)** *Reticulofenestra haqii*: 2795 m depth, well EWW1-St2, Kafr El-Sheikh Fm. **(18)** *Reticulofenestra minuta*: 2615 m depth, well EWE-2, Kafr El-Sheikh Fm. **(19)** *Reticulofenestra perplexa*: 2900 m depth, well EWE-2, Abu Madi Fm. **(20)** *Sphenolithus abies*: 2795 m depth, well EWW1-St2, Kafr El-Sheikh Fm. **(21)** *Sphenolithus moriformis*: 2830 m depth, well EWW1-St2, Abu Madi Fm. **(22)** *Sphenolithus neoabies*: 2788 m depth, well EWW1-St2, Kafr El-Sheikh Fm. **(23)** *Hughesius gizoensis*: 2695 m depth, well EWE-2, Abu Madi Fm. **(24)** *Umbilicosphaera jafari*: 2820 m depth, well EWE-2, Abu Madi Fm. **(25)** *Tetralithoides symeonidesii*: 2640 m depth, well EWE-2, Abu Madi Fm.

NN6 of Martini (1971) and zone CN5a of Okada and Bukry (1980), respectively. Also, the zone corresponds to MNN6a of Fornaciari et al. (1996) and Raffi et al. (2003) for the Mediterranean region.

Age. Middle Miocene (Serravallian).

4.1.9 *Discoaster variabilis* partial zone (CNM9)

Definition. According to Wade et al. (2011) and Backman et al. (2012), this partial range zone corresponds to a body of rock located between the HO of a given taxon and the LO of another taxon. Consequently, we defined the *Discoaster variabilis* zone as a partial range zone comprising the HO of *Calcidiscus premacintyrei* and the LO of *Cyclicargolithus floridanus*.

Occurrence. This zone was recorded only in the Sidi Salem Formation of well EWE-2, encompassing depths from 2990 to 2950 m, with a total thickness of ∼ 40 m (Fig. 7a).

Assemblage. See File 2 in the Supplement.

Remarks. Zone CNM9 (*Discoaster variabilis*) of Backman et al. (2012) corresponds to the upper parts of zones NN6 and CN5a of Martini (1971) and Okada and Bukry (1980), respectively. In the Mediterranean region, this zone is the equivalent of MNN6b of Fornaciari et al. (1996) and Raffi et al. (2003).

Age. Middle Miocene (Serravallian).

4.1.10 *Reticulofenestra pseudoumbilicus* partial range zone (CNM14)

Definition. It comprises the HO of *Discoaster hamatus* and the LO of *Discoaster loeblichii*.

Occurrence. This zone has been recorded only from well EWW1-St2, encompassing a depth from 3300 to 3200 m (100 m thick), within the Sidi Salem Formation (Fig. 7e).

Assemblage. See File 2 in the Supplement.

Remarks. Zone CNM14 (*Reticulofenestra pseudoumbilicus*) of Backman et al. (2012) is correlated with the lower parts of zones NN10 and CN8 (CN8a) of the standard schemes of Martini (1971) and Okada and Bukry (1980) and with MNN10a of Raffi et al. (2003) in the Mediterranean. This zone corresponds to the lowermost part of zone CN8.

Age. Late Miocene (Tortonian).

4.1.11 *Discoaster bellus* interval zone (CNM15)

Definition. This zone was defined as the interval from the LO of *R. pseudoumbilicus* to the LO of *Discoaster berggrenii*.

Occurrence. This interval zone has only been recorded in well EW-5 and encompasses a depth interval from 3300 to 3200 m (100 m thick) within the Sidi Salem Formation (Fig. 7d).

Assemblage. See File 2 in the Supplement.

Remarks. Zone CNM15 (*Discoaster bellus*) of Backman et al. (2012) corresponds to the upper part of zones NN10, CN8, and MNN10b of Martini (1971), Okada and Bukry (1980), and Raffi et al. (2003), respectively.

Age. Late Miocene (Tortonian).

4.1.12 *Amaurolithus primus* interval zone (CNM17)

Definition. This zone was drawn from the LO of *Amaurolithus primus* to the LO of *Nicklithus amplificus*.

Occurrence. Zone CNM17 is recorded in wells EWE-2 (from 2950 to 2820 m), EW-8 (from 3120 to 2930 m), EW-12 (from 3105 to 2815 m), EW-5 (from 3100 to 2883 m), and EWW1-St2 (from 3200 to 2850 m), corresponding to Qawasim and Abu Madi formations. The thickness of this zone is 130, 190, 290, 217, and 350 m, respectively (Fig. 7a–e).

Assemblage. See File 2 in the Supplement.

Remarks. Zone CNM17 (*Amaurolithus primus*) of Backman et al. (2012) is comparable to the middle part of zone NN11 of Martini (1971) and to the lower part of zone CN9b of Okada and Bukry (1980). In the Mediterranean region, this zone corresponds to zone MNN11b of Raffi et al. (2003).

Age. Late Miocene (Messinian).

4.1.13 *Nicklithus amplificus* total range zone (CNM18)

Definition. This zone corresponds to the total range of *N. amplificus*.

Occurrence. This zone is recorded in wells EWE-2 (from 2820 to 2630 m), EW-8 (from 2930 to 2670 m), EW-12 (from 2815 to 2725 m), EW-5 (from 2883 to 2660 m), and EWW1-St2 (from 2805 to 2850 m) and corresponds to the Qawasim and Abu Madi formations. The thickness of this zone is 190, 260, 90, 223, and 45 m, respectively (Fig. 7a–e).

Assemblage. See File 2 in the Supplement.

Remarks. Zone CNM18 (*Amaurolithus primus*) of Backman et al. (2012) corresponds to the upper parts of zone NN11 of Martini (1971) and subzone CN9b (*Amaurolithus primus*) of Okada and Bukry (1980). It is the equivalent of MNN11c defined by Raffi et al. (2003) in the Mediterranean region.

Age. Late Miocene (Messinian).

4.1.14 *Ceratolithus armatus* total range zone (CNPL1)

Definition. This zone comprises the total range of *C. armatus*.

Occurrence. Zone CNPL1 was recognized in wells EWE-2 (from 2630 to 2615 m), EW-8 (from 2670 to 2665 m), EW-12 (from 2725 to 2717 m), and EWW1-St2 (from 2805 to 2788 m), corresponding to the Kafr El-Sheikh Formation. Thus, the thickness of this zone is 15, 5, 8, and 17 m, respectively (Fig. 7a–c and e).

Assemblage. See File 2 in the Supplement.

Remarks. Zone CNPL1 (*Ceratolithus armatus*) of Backman et al. (2012) belongs to the upper part of zone NN12 of Martini (1971) and subzone CN10b of Okada and Bukry (1980).

Age. Early Pliocene (Zanclean).

4.1.15 *Sphenolithus neoabies* partial range zone (CNPL2)

Definition. It is a partial range between the HO of *C. armatus* and the lowest common occurrence (LCO) of *Discoaster asymmetricus*.

Occurrence. Zone CNPL2 was recorded in wells EWE-2 (from 2615 to 2565 m), EW-8 (from 2665 to 2630 m), EW-12 (from 2717 to 2570 m), EW-5 (from 2650 to 2470 m), and EWW1-St2 (from 2788 to 2760 m), corresponding to the Kafr El-Sheikh Formation. At these intervals, the thick-

ness of this zone is 50, 35, 147, 180, and 28 m, respectively (Fig. 7a–e).

Assemblage. See File 2 in the Supplement.

Remarks. Following Backman et al. (2012), we consider zone CNPL2 (*Sphenolithus neoabies*) to be consistent with zone NN13 of Martini (1971) and with subzones CN10c and CN11a of Okada and Bukry (1980).

Age. Early Pliocene (Zanclean).

4.1.16 *Discoaster asymmetricus*/*Reticulofenestra pseudoumbilicus* concurrent range zone (CNPL3)

Definition. The zone is defined based on the consecutive occurrence of the lowest common occurrence of *D. asymmetricus* and the HO of *R. pseudoumbilicus*.

Occurrence. Zone CNPL3 was recorded in wells EW-8 (from 2630 to 2585 m), EW-12 (from 2570 to 2550 m), and EW-5 (from 2470 to 2460 m), corresponding to the Kafr El-Sheikh Formation. The corresponding thickness is 45, 20, and 10 m, respectively (Fig. 7b–c and e).

Assemblage. See File 2 in the Supplement.

Remarks. Zone CNPL3 of Backman et al. (2012) encompasses NN14 and NN15 of Martini (1971) and corresponds to subzone CN11b of Okada and Bukry (1980).

Age. Early Pliocene (Zanclean).

4.2 Palaeoenvironmental reconstruction

The integration of the foraminifera and calcareous nannofossil assemblages allowed reconstruction of the palaeoenvironmental conditions in the study area based on proxies such as benthic foraminiferal depth indicators, P/B ratio, species richness and abundance, and calcareous nannofossil taxa characteristics of peculiar environmental conditions.

In the Serravallian, the occurrence of the calcareous nannofossil *C. floridanus* is reported by some authors to indicate open-marine conditions (Wei and Wise, 1990; Aubry, 1992; Monechi et al., 2000). The benthic foraminiferal association which occurred in this time interval (see File 1 in the Supplement) and is illustrated in Fig. 10 suggests a middle- to outer-neritic environment (Murray, 1991; Holbourn et al., 2013). This result suggests that the depositional environment for the Sidi Salem Formation during the Serravallian was an open shelf (middle- to outer-neritic).

In the Tortonian, the calcareous nannofossils are characterized by the increasing percentage of *Discoaster* taxa, which indicate deep-marine, stable environments (Gibbs et al., 2004; Villa et al., 2008; Athanasiou et al., 2021). The occurrence of benthic assemblages including *O. umbonatus* and *P. bulloides* suggests open-shelf conditions (Fig. 10; Murray, 1991, 2006). This observation confirms the outer-neritic (shelf) depositional environment of the Tortonian Sidi Salem Formation.

In the Messinian, the calcareous nannofossil assemblages were dominated by *Sphenolithus* spp. and by small reticulofenestrids, along with a reduced *Discoaster* percentage and the sporadic occurrence of *A. beccarii*. The occurrence of rare ostracod shells might indicate marginal estuarine conditions, as suggested by Wade and Bown (2006) and Chakraborty et al. (2021).

In the Early Pliocene (Zanclean), a peak in abundance of calcareous nannofossils and foraminifera (both benthic and planktonic) is recorded in the studied cores. A marked increase in the *Discoaster* percentage might indicate an open-marine environment (Chakraborty et al., 2021). This interpretation is further supported by the occurrence of planktonic foraminifera such as *Sphaeroidinellopsis* spp. that are also considered to be open-marine taxa (Wei et al., 1992; Iaccarino et al., 2007). Such conditions are consistent with a global sea-level rise already suggested by Snedden and Liu (2010). Warm-water indicators, such as *C. armatus*, *C. cristatus*, *O. universa*, and *Globigerinoides* spp. (Sinaci, 2013; Verducci et al., 2009), are also recorded in the earliest Zanclean. Consequently, calcareous nannofossil and foraminifer records might confirm that the Kafr El-Sheikh Formation was deposited under open-marine conditions.

4.3 Sequence stratigraphy

Our high-resolution biostratigraphic investigation allows determination of the depositional sequences and system tracts of the Neogene sediments of the Nile Delta system. Facies types are also characterized using a detailed lithologic description incorporated with wireline logs analysis. The use of CycloLog software to generate PEFA and INPEFA patterns has enabled sequence identification (Nio et al., 2005). Many criteria, such as biozonal breaks and subaerial exposures, have been used to inspect sequence boundaries, whereas palaeobathymetry was used to clarify system tracts based on benthic biofacies, planktonic–benthic ratio, abundance, and diversity. Several studies have shown the usefulness of these parameters (e.g. Armentrout, 1996; Leckie and Olson, 2003; Miller et al., 2008). Biostratigraphy allowed the dating of flooding and maximum flooding events. The ages of these events were calibrated with the Neogene timescale of Backman et al. (2012) and Lourens et al. (2004) by using the marker species of both calcareous nannofossils and planktonic foraminifera. The flooding events and depositional sequences have been recognized and correlated with the global cycle chart adopted by Snedden and Liu (2010). Also, the sequence boundaries of this study were correlated with those published for the Nile Delta and the Mediterranean by Dolson et al. (2005), Kellner et al. (2009), and Farouk et al. (2014); other regional sequence boundaries are shown by Haq et al. (1987), Hardenbol et al. (1998), and Wornardt (1999) (Fig. 11). The investigated succession has been subdivided into seven major third-order depositional sequences, bounded by six sequence boundaries related to eu-

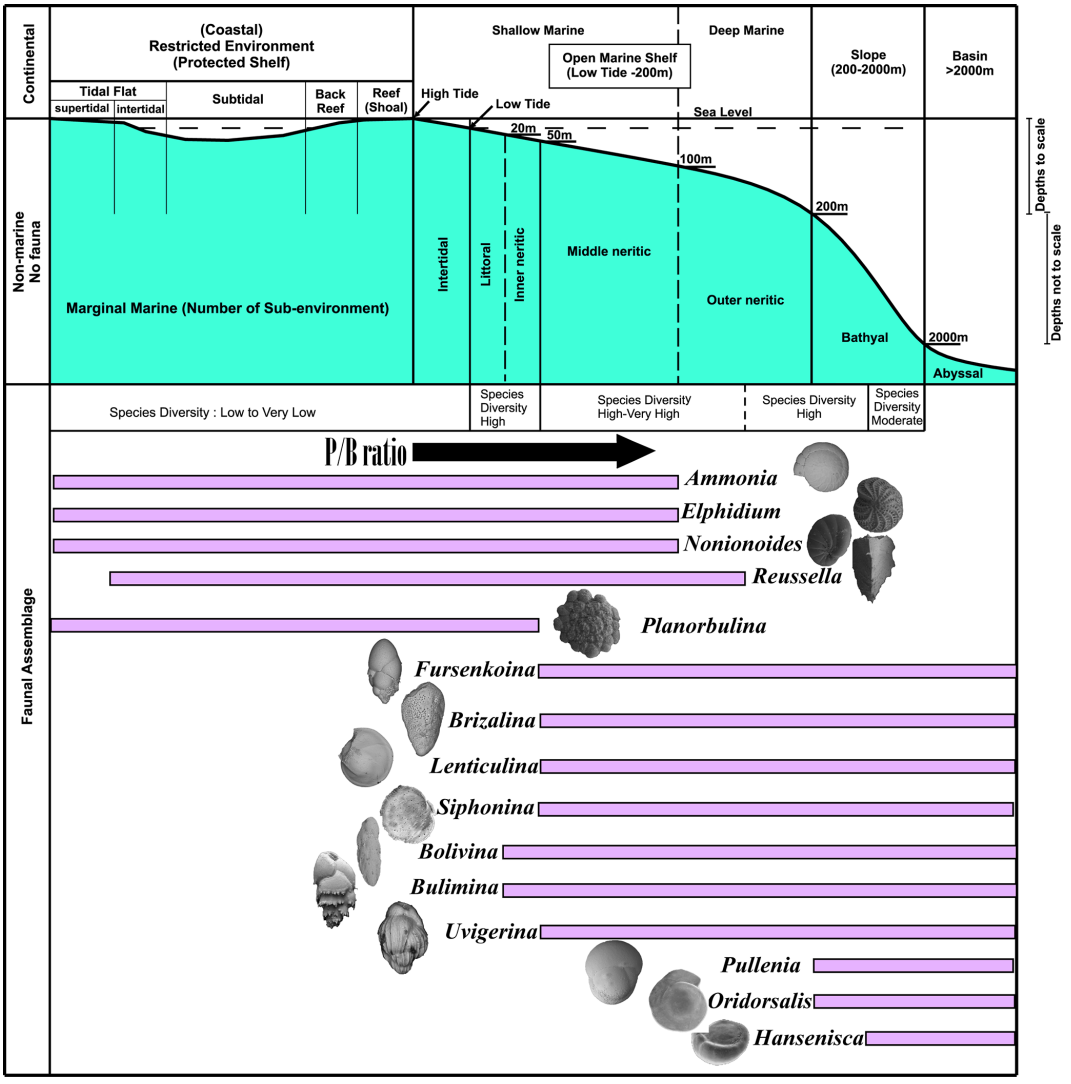

Figure 10. Upper depth limit of benthic foraminifera with respect to P/B ratio after Van Morkhoven et al. (1986), Van der Zwann et al. (1990), Murray (1991), and Holbourn et al. (2013).

static sea-level changes and/or local tectonics. This is based on the results of the integration between wireline logging, seismic data, and high-resolution biostratigraphic data.

4.4 Sequence boundaries of El-Wastani field

Figure 7 shows six sequence boundaries that were correlated with the global sequences proposed by Snedden and Liu (2010) (see File 3 in the Supplement). The unconformity surfaces could be regarded as sequence boundaries (SBs) (Kassab et al., 2015), which define seven depositional sequences in our study area. These sequence boundaries are unconformity surfaces related to subaerial exposure named type 1, such as SB1, SB2, SB3, SB4, and SB5, or submarine erosional unconformity named type 2, such as SB6, as shown in Fig. 7 and File 3 in the Supplement.

The upper SB of the Serravallian sequence (Serseq) is an erosive unconformity surface of type 1 (SB1), which could be dated to 12.18 Ma through correlation with the paper of Kellner et al. (2009). The lower SB could be correlated with the previously defined SB at 12.70 Ma as published by Hardenbol et al. (1998) and Kellner et al. (2009) (Fig. 11).

The upper SB (SB2) of the first Tortonian sequence (Torseq1) is represented by an erosional surface and angular unconformity due to uplift, forming a biostratigraphic break in well EWW1-St2, and could be correlated with the SB at 8.8 Ma identified by Wornardt (1999); the top of this sequence is a maximum flooding surface (MFS). The lower SB of the Torseq1 was not reached in our study, but it might be attributed to the SB described by Hardenbol et al. (1998) and Kellner et al. (2009) at 9.26 Ma (Fig. 11).

The upper SB of Torseq2 (SB3) is characterized by an angular unconformity between the tilted blocks of the Sidi Salem Formation and the overlying Qawasim Formation, as shown in the seismic section of well EW-5 (Fig. 11). The lower SB of Torseq2 was not reached; however, it may be correlated with the sequence boundary defined by Wornardt (1999) at 8.60 Ma (Fig. 11).

The upper SB (SB4) of the first Messinian sequence (Meseq1) is characterized by local unconformity inferred from the incised valley truncation by fluvial input in the lower Abu Madi Formation, as shown by the NNE–SSW-trending seismic line that crosses the valley direction (NNW–SSE) (Fig. 12a–b). The Meseq1 upper SB (local unconformity) is observed in all the studied wells and could be correlated with the SB identified by Hardenbol et al. (1998) and Kellner et al. (2009) at 6.98 Ma. The lower SB was not reached in wells EW-8 and EW-12, but it could be correlated with the SB at 7.24 Ma defined by Farouk et al. (2014) in the Nile Delta (Fig. 11).

The upper SB of sub-cycle Meseq2a represents another phase of valley incision, which truncated older beds, as shown by seismic sections (Fig. 12a–b). The upper SB (SB5) of Meseq2 corresponds to a type 1 erosive surface due to subaerial erosion (zones CNM19 and CNM20), dated to the latest Messinian.

The upper SB (SB6) is a submarine erosive surface (type 2), as indicated by lithofacies and gamma-ray signals. This SB is correlated with the ones recognized at 4.36 Ma by Hardenbol et al. (1998) and Kellner et al. (2009) and at 4.37 Ma by Snedden and Liu (2010) (Fig. 11).

4.5 Depositional sequences of El-Wastani field

The five studied wells contain seven depositional sequences encompassing the Serravallian to Zanclean periods (Fig. 7). These are Serseq1, Torseq1, Torseq2, Meseq1 $(a+b)$, Meseq2 $(a+b)$, Zaseq1, and Zaseq2. The description of each depositional sequence and sequence boundary in the five wells is as follows.

I. Serravallian sequence (Serseq)

The lowermost Miocene depositional sequence (Serseq) occurs in the Sidi Salem Formation and corresponds to foraminiferal subzone MMi7b and calcareous nannofossil zones CNM8 and CNM9. Serseq is recorded in well EWE-2 (Fig. 7a). Serseq is composed of shale beds that reflect an open-shelf (middle- to outer-neritic) environment as inferred from benthic foraminifer and calcareous nannofossil contents (Fig. 7). It corresponds to retrograding parasequences defining the TST (transgressive system tract). A gap occurred corresponding to the uppermost Serravallian–lower Tortonian sequences, as also shown by the absence in the studied well of some foraminiferal zones (MMi8, MMi9, MMi10), as well as of some calcareous nannofossil zones (CNM8 to CNM13).

SB1 is marked by a long hiatus occurring between the Serravallian Sidi Salem and the overlying Messinian Qawasim formations. The regional tectonic uplift of the Serravallian tilted blocks in the eastern part of Africa was the main driver for this hiatus, easily seen in the seismic profile (Harms and Wary, 1990). A shift occurs in the depositional environment, from middle- to outer-neritic deposits in the Serravallian to fluvial–marine and lagoon facies of the Messinian age, as inferred from the rare and poorly diversified benthic foraminifera (see File 1 in the Supplement). Subzone MMi7b and nannofossil zones CNM8 and CNM9 are recorded below SB1. The latter surface is overlain directly by the Messinian NDZ and by zones CNM17 and CNM18. The hiatus and the observed change in environmental conditions were likely driven by local tectonics in the Nile Delta area due to the rifting in the Gulf of Suez (Farouk et al., 2014).

The TST is characterized by the deposition of middle- to outer-neritic shales, rich in foraminifera and calcareous nannofossils (subzone MMi7b, zones CNM17 and CNM18), because of a relative sea-level rise. The foraminiferal assemblages show a $P/(P+B)$ ratio of 39 % to 67 %, high species richness (25–36), and a moderate to good preservation state (see File 1 in the Supplement).

II. First Tortonian sequence (Torseq1)

This sequence is recorded in well EWW1-St2 (Fig. 7e). It corresponds to the upper Sidi Salem Formation (zone MMi11 and the lower part of zone CNM14). The Torseq1 is characterized by a regional angular unconformity between the tilted blocks of the Sidi Salem Formation and the Qawasim Formation, as shown by the NW–SE seismic section (Fig. 12a–b) and previously inferred for the Nile Delta by El-Heiny and Morsi (1992). Torseq1 corresponds to a TST made of retrograding parasequences (Fig. 7e).

The TST is composed of middle- to outer-neritic shales yielding high planktonic foraminiferal and calcareous nannofossil contents. This interval shows a $P/(P+B)$ ratio of $\sim$76 % and moderate to high foraminiferal diversity (benthic and planktonic, $\sim$17 species), with moderate to good preservation. The benthic foraminiferal assemblage comprises deep-water taxa (see File 1 in the Supplement). High abundance and diversity of calcareous nannofossils are also observed in the TST interval.

III. Second Tortonian sequence (Torseq2)

It is recorded in well EW-5 (Fig. 7d) and encompasses the uppermost Sidi Salem Formation (zone MMi11, zone CNM15). The top of Torseq2 occurs near the Tortonian–Messinian boundary and is accompanied by significant change in foraminiferal assemblages, which shift from moderate to high abundances to a barren interval. Some plank-

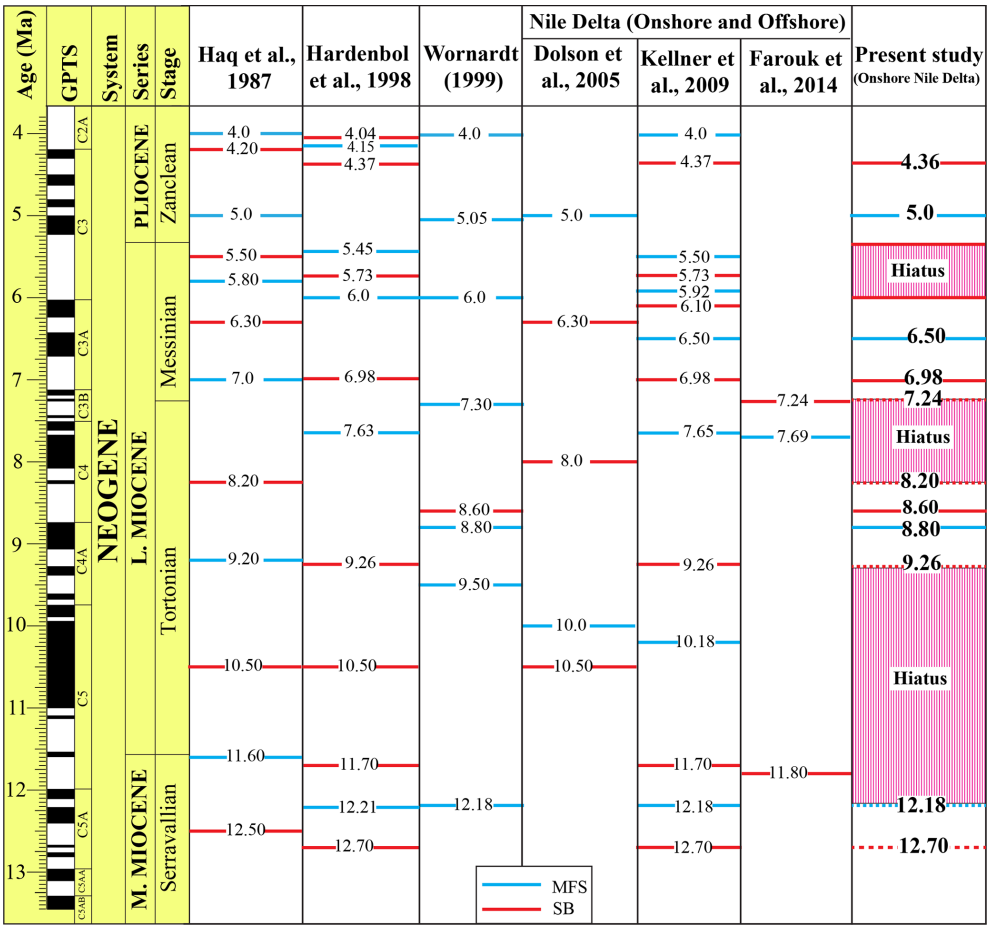

Figure 11. Sequence stratigraphic boundaries of the onshore Nile Delta in comparison with global and other related geographical regions. Chronostratigraphic scale after Ogg et al. (2016).

tonic foraminiferal and calcareous nannofossil zones are missing, namely MMi11 to MMi13 and CNM17 to CNM18. Torseq2 contains only the highstand system tract (HST) prograding parasequences.

The HST is composed of inner- to middle-neritic shale yielding moderately abundant and diversified planktonic foraminifera and calcareous nannofossils. It is characterized by a $P/(P+B)$ ratio of $\sim$45 %, with a moderate foraminiferal diversity (benthic and planktonic, 8–17 species) and a moderate preservation state (see File 1 in the Supplement).

IV. First Messinian sequence (Meseq1)

It corresponds to the lowermost Messinian Qawasim Formation in the five studied wells (Fig. 7) and to zones NDZ and CNM17. The Meseq1 sequence comprises the lowstand system tract (LST)/TST and HST as retrograding/prograding and aggrading parasequences. It is well represented in well EW-12 (Fig. 7c).

The LST is a prograding sedimentary body, as shown by the deposits of the lower Messinian Qawasim succession. Lithofacies are mainly composed of sandy deposits with grains of variable size, corresponding to a submarine canyon formed in the context of sea-level drop. These LST deposits are well recognized in well EW-8 (Fig. 7c). An interval barren in planktonic and benthic foraminifera and with low to moderate calcareous nannofossil abundance was observed in some wells (EW-8, EW-12, EWW1-St2) (see Files 1 and 2 in the Supplement).

The TST is dominated by sands with shale interbeds. The TST deposits occur in the five wells (EWE-2, EWW1-St2, EW-5, EW-8, EW-12). Calcareous nannofossils show a trend of increasing abundance upward, whereas only shallow benthic foraminifera are recorded (see Files 1 and 2 in the Supplement).

The MFS could be placed in the first four wells and represents the maximum abundance and diversity of the calcareous nannofossils. The overlying HST deposits exhibit low to moderate nannofossil abundances.

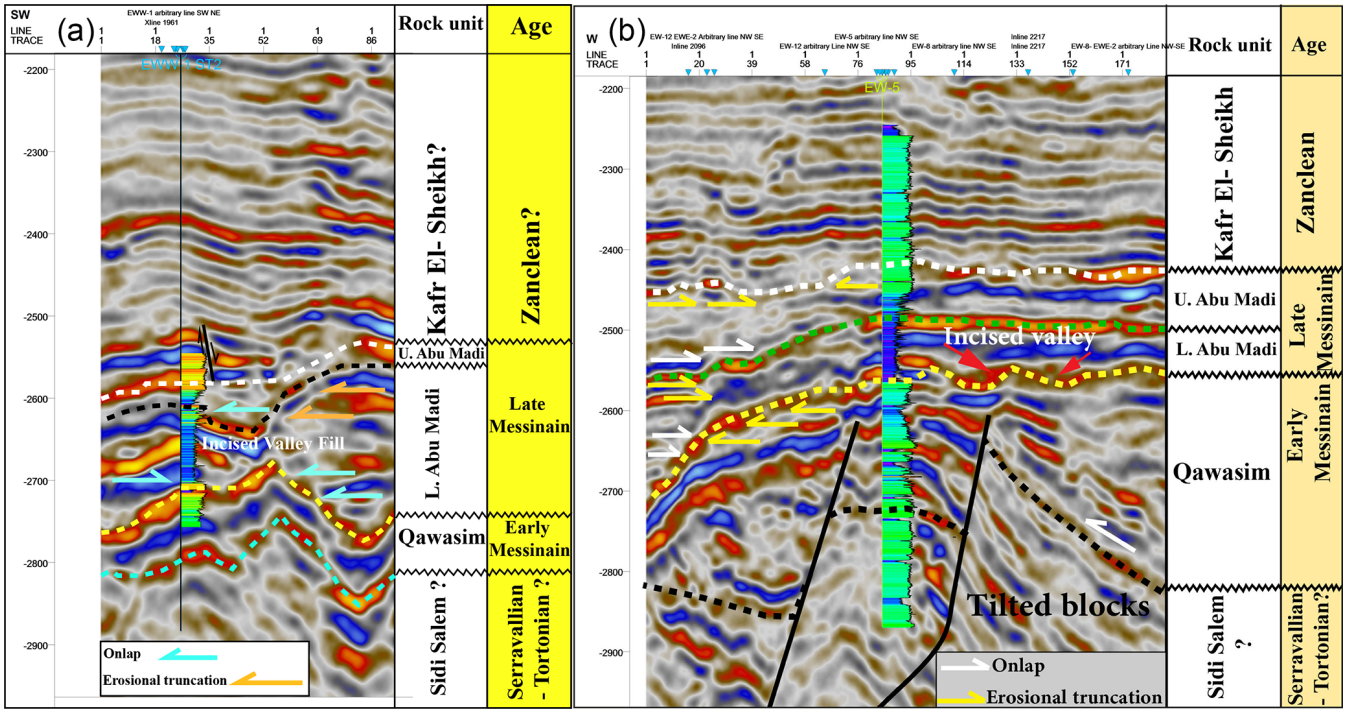

Figure 12. NE–SW seismic-to-well-tie profile illustrating the rock units, stratum terminations, and stratigraphic boundary of each rock unit of wells EWW1-St2 and EW-5 in the El-Wastani gas field.

V. Second Messinian sequence (Meseq2)

It is recorded in wells EWW1-St2, EWE-2, EW-5, EW-8, and EW-12 and corresponds to the calcareous nannofossil zones CNM17 and CNM18 and to the uppermost part of the foraminiferal NDZ of the Abu Madi Formation. The Meseq2 depositional sequence is composed of two sub-cycles, Meseq2a and Meseq2b (Fig. 7). The lower and upper SBs of the Meseq2a and Meseq2b sub-cycles present multiple phases of valley incision and truncation of the beds (Fig. 12a–b). Due to such features, reworked calcareous nannofossils commonly occur in the sediments at the base of each sub-cycle.

According to Catuneanu et al. (2011), the LST follows a regressive sequence, which deposited at the beginning of sea-level drop and the subsequent relative sea-level rise. The fluvial–deltaic system throughout the delta region is represented by a prograding, lowstand clastic unit (Abu Madi Fm.), which is interpreted as having deposited during sea-level fall (Abdel Hady et al., 2013). High percentages of reworked microfossils (from Cretaceous, Palaeogene, and Neogene) are recorded in the Messinian Abu Madi Fm. Catuneanu et al. (2011) showed that the infilling of incised valleys began in the final stage of the LST. In the five studied wells, the lowstand facies in the two sub-cycles of Meseq2 represent the thickest part of the entire sequence, being composed of a sandstone unit (Fig. 7). Because of its porosity, the LST of the Abu Madi Fm. represents the most important Miocene gas reservoir in the Nile Delta system.

The TST is dominated by shales and sand interbeds, as shown by the gamma-ray signal and INPEFA log pattern (Fig. 7). Also, a slight increase in the calcareous nannofossil abundance occurs during the retrograding parasequences. Conversely, planktonic foraminifera are absent, and only *A. beccarii* characterizes the benthic forms. The TST facies occur in the five investigated wells, in both the Meseq1a and Meseq2b (Fig. 7).

The Meseq2b MFS has been tentatively placed at the top of the transgressive sequence based on the record of high calcareous nannofossil abundances and diversity. The overlying regressive sequence (HST) contains slightly fewer calcareous nannofossils and some shallow-water benthic foraminifers such as *Elphidium* sp. and *A. beccarii*.

VI. First Zanclean sequence (Zaseq1)

Zaseq1 is the oldest Pliocene depositional sequence that comprises the Kafr El-Sheikh Formation and spans zones MPl1 and MPl2 and the lower part of zone MPl3, correlated with calcareous nannofossil zones CNPL1 and CNPL2.

The TST is placed in the lower part of the Kafr El-Sheikh Formation (zones MPl1, MPl2, and CNPL1). The TST retrograding facies is recorded from four wells (EWW1-St2, EWE-2, EW-8, and EW-12), as shown by gamma-ray signals and INPEFA log patterns (Fig. 7). The highest abundance

and species diversity of both planktonic foraminifera and calcareous nannofossils are observed in Zaseq1. The high occurrence of deep-water benthic foraminifer indicators (see File 1 in the Supplement) suggests an outer-neritic–upper-bathyal environment, also compatible with a $P/(P+B)$ ratio up to 95 %.

The MFS is identified within the Kafr El-Sheikh Formation in four wells (Fig. 7). This surface corresponds to the highest abundance of planktonic and benthic foraminifera and calcareous nannofossils. Foraminifera specimens are coated by pyrite, whose formation is compatible with dysoxic conditions within the sediment. The MFS is correlated with the analogous event described by Haq et al. (1987) and Dolson et al. (2005) at 5.0 Ma and by Wornardt (1999) at 5.05 Ma (Fig. 11). The MFS of Zaseq1 is thus one of the most relevant surfaces near the top of zone MPl1 and the calcareous nannofossil zone CNPL1 at 5.0 Ma.

The HST facies is recorded from all five wells (Fig. 7). The HST is composed of neritic shale, with few sands and silt interbeds. The interpretation of electric logs and CycloLog data suggests the occurrence of a continuous sea-level fall and a change from deep, open-marine facies to middle- and outer-neritic environments. The $P/(P+B)$ ratio shows values of 53 %–68 %, with a moderate to high species diversity of foraminifera and calcareous nannofossils, as well as a good preservation of benthic forms.

VII. Second Zanclean sequence (Zaseq2)

This depositional sequence occurs in wells EW-5 and EW-12 (Fig. 7) in the lowermost part of the Kafr El-Sheikh Formation. In well EW-5, the depositional sequence is dated to the upper part of MPl3 and the calcareous nannofossil zone CNPL3. Well EW-12 corresponds to the upper part of zones MPl2 and CNPL3.

The LST/TST interval in the Kafr El-Sheikh Formation is composed of light to brownish-grey shales with traces of organic matter. The $P/(P+B)$ ratio is 45 %–67 %, with an upwards increase in relative abundance and species diversity of both foraminifera and calcareous nannofossils. Benthic foraminifera are dominant in this interval (see File 1 in the Supplement) and suggest deposition in an inner- to middle-neritic environment.

4.6 Correlation of the depositional sequences with previous works

The Middle–Late Miocene (Serravallian/Tortonian) boundary is characterized by a small-amplitude sea-level fall in the Tethyan realm (Hardenbol et al., 1998; Snedden and Liu, 2010). In the Serravallian, the eastern part of Egypt was affected by tectonic activity (Dolson et al., 2001). This caused uplift and tilting to the north of the older rock units. Accordingly, the oldest Serravallian sequence (Serseq) is only recorded in well EWE-2, corresponding to the south-eastern part of the El-Wastani field (Fig. 7). This tectonic activity is responsible for a long hiatus between the Serravallian sequence, which is lacking in the northern wells, and the overlying Messinian sequence. The Serseq sequence is interpreted here as being made of TST deposits. This interpretation is in contradiction to Farouk et al. (2014), who interpreted HST facies for the same interval. On the north-western side of the study area, wells EWW1-St2 and EW-5 are composed of Tortonian sediments. Both wells were affected by tectonic activity that occurred in the Serravallian, hence creating the upper SBs of Torseq1 and Torseq2. The two Tortonian sequences are correlated with the ones recorded by Farouk et al. (2014), even though these authors interpreted the lower part of the sequence as an LST.

During the Messinian time, the drawdown of the Mediterranean and, in turn, of the Nile Delta incised channels cut the upper parts of the Serravallian–Tortonian Sidi Salem Formation; such channels were infilled by the Qawasim unit (Meseq1). The sequence thickness increases in the central part of the field (well EW-8), which may represent the deepest part of the channel, in agreement with Farouk et al. (2014). The Abu Madi Formation was formed under the influence of multiphases of fluvial channels cut, which form the upper SB of Meseq2. The thickness of Meseq2 is important along the margin of the field; thus the main channel pass was likely located between wells EWW1-St2 and EWE-2, whereas minor channels occurred in the central field. Meseq2 is also recorded by Farouk et al. (2014) in the same time interval.

The lowermost Zanclean (Zaseq1, Kafr El-Sheikh Formation) likely corresponds to the first arrival of marine water from the Atlantic Ocean through the Gibraltar seaway (Roveri et al., 2014) (Fig. 7). This sequence corresponds to TST/HST in four of the investigated wells, excluding EW-5, which only bears a HST due to the lack of zone MPl1 and zone CNPL1. This lack may be due to the rarity of the zonal markers in well EW-5. The Zaseq1 thickness is important in wells EW-5 and EW-12, probably due to fault initiation in the Pliocene (Kamel et al., 1998) or because the deepest part of the basin was located around these wells. Well Zaseq1 matches with the sequence reported by Farouk et al. (2014).

4.7 Sequence stratigraphy and hydrocarbon potential

In the present work, the analysis of the lower and upper Messinian rock units (Qawasim and Abu Madi formations) in the framework of a sequence stratigraphy study allows an effective correlation for exploration with other onshore concessions of the Nile Delta. The LSTs correspond to the most important gas reservoirs due to the occurrence of sandstone deposits (Catuneanu et al., 2011). These thick sandstone units have been observed in the LST of the Meseq1 and Meseq2 of the Messinian Qawasim and Abu Madi formations of the present study. Hydrocarbon occurrence in a lowstand sequence is influenced by charge, seals, and source

rocks. According to Catuneanu et al. (2011), fluvial, coastal, and shallow-water lowstand reservoirs are sealed by overlying evaporite layers and transgressive shales. In the El-Wastani field, three prograding lowstand wedges were identified, two belonging to the Abu Madi Formation and the third one belonging to the Qawasim Formation, based on our high-resolution biostratigraphy and geophysical log patterns. The LST deposits are sealed by marine shales. The Messinian channel infilling (Qawasim and Abu Madi Fm.) in a bounded-fault context, locally bearing unconformities due to occurrence of fluvial channels, acted as stratigraphic traps (Fig. 12a, b). The MFS deposits may have acted as source rocks for hydrocarbon generation (Dolson et al., 2002).

5 Conclusions

A detailed biostratigraphic study based upon planktonic and benthic foraminifera and calcareous nannofossils was conducted in five wells located within the El-Wastani field, onshore Nile Delta, Egypt, and allowed identification of Middle Miocene–Early Pliocene sequences. Six biozones based on planktonic foraminifera markers and nine biozones based upon calcareous nannofossils were established. These allowed correlation with the most relevant Miocene–Pliocene biozonal schemes from the Mediterranean region and middle latitudes. Benthic foraminifera and calcareous nannofossil assemblages were used to reconstruct depositional environments, which range from lagoon to upper-bathyal environments. The integration of sequence stratigraphy, wireline logs (gamma rays), and biostratigraphy allowed the identification of seven depositional sequences. These sequences highlighted the reservoir-bearing intervals of the Qawasim and Abu Madi formations that proved to be incised valleys over older rock units, as shown by the NE–SW seismic lines. Our study will enable the future exploration in the Nile Delta provinces.

Appendix A: Taxonomic list of the species recorded in this study

Planktonic foraminifera

Globoturborotalita nepenthes Todd, 1957, Figs. 2.1–2.2
Globigerina bulloides d'Orbigny, 1826, Figs. 2.3–2.6
Globigerina falconensis Blow, 1959, Figs. 2.7–2.8
Trilobatus sacculifer Brady, 1877, Figs. 2.9–2.10
Globigerinoides conglobatus Brady, 1879, Fig. 2.11
Trilobatus trilobus Reuss, 1850, Figs. 2.12–2.15
Orbulina universa d'Orbigny, 1839, Figs. 2.16–2.19

Recently Brummer and Kucera (2022) invalidated the basionym of *O. bilobata*, which became *O. universa*. Consequently, we consider in our paper the species *O. universa*.

Orbulina suturalis Brönnimann, 1951†, Fig. 2.20
Globigerinoides obliquus Bolli, 1957, Figs. 2.21–2.24
Globigerinoides extremus Bolli and Bermudez, 1965, Figs. 3.1–3.2
Paragloborotalia mayeri Cushman and Ellisor, 1939, Figs. 3.3–3.4

The specimens illustrated possess five inflated chambers. The first chamber is small and clearly apparent in ventral view. The spiral suture is slightly curved and depressed. These specimens display an increasing chamber size, which is characteristic of the Middle Miocene *P. mayeri*. These criteria are compatible with the holotype description of *P. mayeri*.

Globorotalia margaritae Bolli and Bermudez 1965, Fig. 3.5–3.6
Globoconella puncticulata Deshayes, 1832, Figs. 3.7–3.8
Sphaeroidinellopsis seminulina Schwager, 1866, Figs. 3.9–3.10
Sphaeroidinellopsis paenedehiscens Blow, 1969, Figs. 3.11–3.13
Globigerinella siphonifera d'Orbigny, 1839, Figs. 3.14–3.15
Neogloboquadrina acostaensis Blow, 1959, Figs. 3.16–3.17
Paragloborotalia continuosa Blow, 1959, Figs. 3.18–3.19

These specimens are only composed of four chambers. The test is globular, and in umbilical view, the chambers are strongly inflated, with sutures slightly depressed, while the umbilicus is narrow and moderately deep. The aperture is moderately high, with a comma-shaped arch, and bordered by a narrow, thick, and continuous lip. Spirally, the test is flattened and broadly rounded in the periphery. These criteria are compatible with the holotype description. The last whorl of *Neogloboquadrina acostaensis* (Figs. 4.6–7) consists of five chambers and is totally different from *P. continuosa*. The test is strongly lobulate equatorially, and chambers are inflated and subspherical to ovate in shape. The sutures on the spiral and umbilical sides are depressed. The umbilicus is narrow and deep, while the aperture is interio-marginal and extraumbilical–umbilical. Consequently, the specimens in Figs. 8–9 in this paper are attributed to *P. continuosa*, while specimens in Figs. 4.6–7 belong to *N. acostaensis*.

Trilobatus immaturus LeRoy, 1939, Figs. 3.20–4.21
Globigerinella obesa Bolli, 1957, Figs. 3.21–3.22
Globigerinoides ruber d'Orbigny, 1839, Fig. 3.24

Benthic foraminifera

Textularia pseudorugosa Lacroix, 1931, Fig. 4.1
Textularia sp. 1, Fig. 4.2
Textularia sp. 2, Fig. 4.3
Martinottiella communis d'Orbigny, 1846, Figs. 4.4–4.5
Quinqueloculina sp., Fig. 4.6
Elphidium sp., Figs. 4.7–5.8
Ammonia beccarii Linnaeus, 1758, Figs. 4.9–4.11
Nonionoides turgidus Williamson, 1858, Figs. 4.12
Lenticulina calcar Linnaeus, 1758, Fig. 4.13

Lenticulina inornata d'Orbigny, 1846, Fig. 4.14
Heterolepa praecincta Karrer, 1868, Figs. 4.15–4.16
Hansenisca soldanii d'Orbigny, 1826, Figs. 4.17–4.18
Planorbulina mediterranensis d'Orbigny, 1826, Fig. 4.19
Pullenia bulloides d'Orbigny, 1846, Figs. 4.20–4.21
Sphaeroidina bulloides d'Orbigny, 1826, Figs. 4.22–4.23
Epistomaroides sp., Fig. 4.24
Siphonina reticulata Čžjžek, 1848, Fig. 4.25
Nonionella chiliensis Cushman and Kellett, 1929, Fig. 4.26
Oridorsalis umbonatus Reuss, 1851, Fig. 4.27–4.29
Uvigerina peregrina Cushman, 1923, Figs. 5.1–5.2
Uvigerina semiornata d'Orbigny, 1846, Fig. 5.3
Rectuvigerina sp., Fig. 5.4
Uvigerina striatissima Perconig, 1955†, Fig. 5.5
Oolina laevigata d'Orbigny, 1839, Fig. 5.6
Bolivina dilatata Reuss, 1850, Fig. 5.7
Brizalina striatula Cushman, 1922, Fig. 5.8
Bolivina spathulata Williamson, 1858, Figs. 5.9–5.10
Brizalina sp., Fig. 5.11
Bulimina marginata d'Orbigny, 1826, Figs. 5.12–5.13
Bulimina elongata d'Orbigny, 1846, Fig. 5.14
Bulimina striata d'Orbigny in Guérin-Méneville, 1832, Fig. 5.15
Protoglobobulimina pupoides d'Orbigny, 1846, Fig. 5.16
Fursenkoina seminuda Natland, 1938, Fig. 5.17
Fursenkoina sp., Fig. 5.18
Reussella spinulosa Reuss, 1850, Fig. 5.19

Calcareous nannofossils

Braarudosphaera bigelowii Deflandre, 1947, Fig. 8.1
Calcidiscus premacintyrei Theodoridis, 1984, Fig. 8.2
Discoaster quinqueramus Gartner, 1969, Fig. 8.3
Discoaster exilis Martini and Bramlette, 1963, Fig. 8.4
Discoaster pentaradiatus Tan Sin Hok, 1927, Fig. 8.5
Discoaster variabilis Martini and Bramlette, 1963, Fig. 8.6
Discoaster loeblichii Bukry, 1971, Fig. 8.7
Discoaster surculus Martini and Bramlette, 1963, Fig. 8.8
Discoaster bollii Martini and Bramlette, 1963, Fig. 8.9
Discoaster brouweri Bramlette and Riedel, 1954, Fig. 8.10
Discoaster bellus Bukry and Percival, 1971, Fig. 8.11
Discoaster berggrenii Bukry, 1971, Fig. 8.12
Discoaster asymmetricus Gartner, 1969, Fig. 8.13
Discoaster sp., Fig. 8.14
Calcidiscus leptoporus Loeblich and Tappan, 1978, Figs. 8.15–8.16
Calcidiscus macintyrei Loeblich and Tappan, 1978, Fig. 8.17
Reticulofenestra rotaria Theodoridis, 1984, Fig. 8.18
Ceratolithus cristatus Kamptner, 1950, Fig. 8.19
Ceratolithus armatus Muller, 1974, Fig. 8.20
Helicosphaera sellii Jafar and Martini, 1975, Fig. 8.21
Coronocyclus nitescens Bramlette and Wilcoxon, 1967, Fig. 8.22
Coccolithus miopelagicus Bukry, 1971, Fig. 8.23
Coccolithus pelagicus Schiller, 1930, Fig. 8.24
Amaurolithus primus Gartner and Bukry, 1975, Fig. 8.25
Cyclicargolithus floridanus Bukry, 1971, Fig. 8.26
Helicosphaera carteri Kamptner, 1954, Fig. 8.27
Amaurolithus tricorniculatus Gartner and Bukry, 1975, Fig. 8.28
Rhabdosphaera clavigera Murray and Blackman, 1898, Fig. 8.29
Amaurolithus delicatus Gartner and Bukry, 1975, Fig. 8.30
Helicosphaera intermedia Martini, 1965, Fig. 9.1
Helicosphaera stalis Theodoridis, 1984, Fig. 9.2
Helicosphaera walbersdorfensis Muller, 1974, Fig. 9.3
Helicosphaera orientalis Black, 1971, Fig. 9.4
Scyphosphaera lagena Kamptner, 1955, Fig. 9.5
Scyphosphaera pulcherrima Deflandre, 1942, Fig. 9.6
Scyphosphaera globulata Bukry and Percival, 1971, Fig. 9.7
Scyphosphaera porosa Kamptner, 1967, Fig. 9.8
Scyphosphaera apsteinii Lohmann, 1902, Fig. 9.9
Pontosphaera discopora Schiller, 1925, Fig. 9.10
Pontosphaera multipora Roth, 1970, Fig. 9.11
Pontosphaera japonica Nishida, 1971, Fig. 9.12
Orthorhabdus rugosus Young and Bown, 2014, Fig. 9.13
Orthorhabdus serratus Bramlette and Wilcoxon, 1967, Fig. 9.14
Nicklithus amplificus Raffi, Backman and Rio, 1998, Fig. 9.15
Reticulofenestra pseudoumbilicus Gartner, 1969, Fig. 9.16
Reticulofenestra haqii Backman, 1978, Fig. 9.17
Reticulofenestra minuta Roth, 1970, Fig. 9.18
Reticulofenestra perplexa Wise, 1983, Fig. 9.19
Sphenolithus abies Deflandre in Deflandre and Fert, 1954, Fig. 9.20
Sphenolithus moriformis Bramlette and Wilcoxon, 1967, Fig. 9.21
Sphenolithus neoabies Bukry and Bramlette, 1969, Fig. 9.22
Hughesius gizoensis Varol, 1989, Fig. 9.23
Umbilicosphaera jafari Muller, 1974, Fig. 9.24
Tetralithoides symeonidesii Theodoridis, 1984, Fig. 9.25

Data availability. The datasets used and/or analysed during the current study are included in the published article and the Supplement and are available from the corresponding authors on reasonable request.

Supplement. The supplement related to this article is available online at: https://doi.org/10.5194/jm-42-147-2023-supplement.

Author contributions. NAE, ANEB, and WGK proposed and designed the research study. RMEK contributed to the acquisition of data, analysed the data, and prepared the manuscript with contributions from all co-authors. All authors approved the final version of the paper.

Competing interests. The contact author has declared that none of the authors has any competing interests.

Disclaimer. Publisher's note: Copernicus Publications remains neutral with regard to jurisdictional claims in published maps and institutional affiliations.

Acknowledgements. The authors thank the El-Wastani Petroleum Company (WASCO) and Egyptian General Petroleum Cooperation (EGPC) for providing the samples and permission to publish the data, which were necessary to achieve this work. We also acknowledge the EREX Petroleum Consultants for providing the software. We are grateful to the Micropalaeontological Society and JoM for their assistance in publishing this article as part of the first author's doctoral dissertation. Thanks go to Martin Pickford and Etienne Jaillard, who kindly revised the English of the final paper. The associate editor Emanuela Mattioli and two anonymous reviewers are acknowledged for their constructive comments and suggestions.

Review statement. This paper was edited by Emanuela Mattioli and reviewed by two anonymous referees.

References

Abdel Aal, A. A., El Barkooky, A., Gerrits, M., Meyer, H., Schwander, M., and Zaki, H.: Tectonic evolution of the Eastern Mediterranean Basin and its significance for hydrocarbon prospectivity in the ultradeepwater of the Nile Delta, Leading Edge, 19, 1086–1102, 2000.

Abdel Hady, A., Al Araby, A., and Hassouba, A.: Modeling of Depositional Environment and Sequence Stratigraphy of Abu Madi Reservoir, El Wastani Field, West El Manzala Concession, Onshore Nile Delta, Egypt. M. Sc., 175 pp., 2013.

Abdel-Kireem, M., Abdou, H., and Samir, A.: Pliocene biostratigraphy and paleoclimatology of the Buseili-1x well, Nile Delta, Egypt, Neues Jahrb. Geol. Palaontol. Abh., 10, 577–593, 1984.

Abdou, H., Abdel-Kireem, M., and Samir, A.: Neogene planktonic foraminiferal biostratigraphy of Nile Delta, Geol. Mediterr., 11, 193–205, 1984.

Abdou, H. F., Abdel-Kireem, M. R., and Samir, A. M.: Neogene planktonic foraminiferal biostra-tigraphy of Nile Delta, Geol. Mediterran., 11, 193–205, 1984.

Agnini, C., Monechi, S., and Raffi, I.: Calcareous nannofossil biostratigraphy: historical background and application in Cenozoic chronostratigraphy, Lethaia, 50, 447–463, 2017.

Armentrout, J. M.: High resolution sequence biostratigraphy: examples from the Gulf of Mexico Plio-Pleistocene, Geol. Soc. Spec. Publ., 104, 65–86, 1996.

Athanasiou, M., Triantaphyllou, M. V., Dimiza, M. D., Gogou, A., Panagiotopoulos, I., Arabas, A., Skampa, E., Kouli, K., Hatzaki, M., and Tsiolakis, E.: Reconstruction of oceanographic and environmental 206 conditions in the eastern Mediterranean (Kottafi Hill section, Cyprus Island) during the middle Miocene Climate Transition, Revue de Micropaleìontologie, 70, 100480 https://doi.org/10.1016/j.revmic.2020.100480, 2021.

Aubry, M. P.: Late Paleogene calcareous nannofossils evolution: A tale of climatic deterioration, in: Eocene – Oligocene climatic and biotic evolution, edited by: Prothero, D. R. and Berggren, W. A., Princeton University Press, Princeton, 272–309, https://doi.org/10.1515/9781400862924.272, 1992.

Backman, J., Raffi, I., Rio, D., Fornaciari, E., and Pälike, H.: Biozonation and biochronology of Miocene through Pleistocene calcareous nannofossils from low and middle latitudes, Newsl. Stratigr., 45, 221–244, 2012.

Berggren, W. A., Kent, D. V., Swisher, C. C., and Aubry, M. P.: A revised Cenozoic geochronology and chronostratigraphy, in: Geochronology, time scales and global stratigraphic correlation: A unified temporal framework for an historical geology, edited by: Berggren, W. A., Kent, D. V., Aubry, M.-P., and Hardenbol, J., Spec. Publ. Soc. Econ. Paleontol. Mineral., 54, 29–212, 1995.

Blow, W. H.: Late Middle Eocene to Recent planktonic foraminiferal biostratigraphy, in: Proceedings of the First International Conference Planktonic Microfossils 1967, Geneva, Switzerland, Leiden, E. J. Brill, 1, 199–242, 1969.

Bolli, H. M. and Saunders, J. B.: Oligocene to Holocene low latitude planktic foraminifera, in: Plankton Stratigraphy, edited by: Bolli, H. M., Saunders, J. B., and Perch-Nielsen, K., Cambridge, Cambridge University Press, Cambridge 155–262, https://doi.org/10.1017/S0016756800035214, 1985.

Borsetti, A., Cati, F., Colalongo, M., and Sartoni, S.: Biostratigraphy and absolute ages of the Italian Neogene. Ann. Geol. Hellen., 7th Internat. Congr. Meditt. Neogene, Athens, 183–197, 1979.

Catuneanu, O., Galloway, W. E., Kendall, C. G. S. C., Miall, A. D., Posamentier, H. W., Strasser, A., and Tucker, M. E.: Sequence stratigraphy: methodology and nomenclature, Newsl. Stratigr., 44, 173–245, 2011.

Chakraborty, A., Ghosh, A. K., and Saxena, S.: Neogene calcareous nannofossil biostratigraphy of the northern Indian Ocean: Implications for palaeoceanography and palaeoecology, Palaeogeogr. Palaeocl., 579, 110583, https://doi.org/10.1016/j.palaeo.2021.110583, 2021.

Cita, M. B.: Studi sul Pliocene e gli strati di passaggio dal Miocene al Pliocene, VII. Planktonic foraminifereal biozonation of the Mediterranean Pliocene deep sea record, Riv. Ital. Paleontol. Stratigr., 81, 527–544, 1975.

Dolson, J., Boucher, P., Siok, J., and Heppard, P.: Key challenges to realizing full potential in an emerging giant gas province: Nile Delta/Mediterranean offshore, deep water, Egypt, J. Geol. Soc. London, Petrol. Geol. Conf. series, 6, 607–624, https://doi.org/10.1144/0060607, 2005.

Dolson, J. C., Shann, M. V., Matbouly, S. I., Hammouda, H., and Rashed, R. M.: Egypt in the twenty-first century: petroleum potential in offshore trends, Geoarabia, 6, 211–230, 2001.

Dolson, J. C., Boucher, P. J., Dodd, T., and Ismail, J.: Petroleum potential of an emerging giant gas province, Nile Delta and Mediterranean Sea off Egypt, Oil Gas J., 100, 32–32, 2002.

EGPC: Nile Delta and North Sinai: Fields, Discoveries and Hydrocarbon Potentials (a Comprehensive Overview), Cairo, EGPC 3 pp., ISBN 9781629810683, 1994.

El-Barkooky, A. and Helal, M.: Some Neogene stratigraphic aspects of the Nile Delta proceedings of MOC, 717–754, ISBN 9788894043624, 2002.

El-Heiny, I. and Morsi S.: Stratigraphic correlation of the Neogene sediments in the eastern Nile Delta and Gulf of Suez, Egypt, E. G. P. C. Proceedings 11th Petr. Explor. and Production Conf. EGPC, Cairo, 166–192, ISBN 9781629810683 1992.

El-Heiny, I., Rizk, R., and Hassan, M.: Sedimentological model for Abu Madi reservoir sands, Abu Madi field, Nile Delta, Egypt, Proceedings 10th Petr. Explor. and Production Conf. EGPC, Cairo, 1–37, ISBN 9781629810683, 1990.

El-Kahawy, R. M., Aboul-Ela, N., El-Barkooky, A. N., and Kassab, W.: Biostratigraphy and paleoenvironment implications of the Middle Miocene-Early Pliocene succession, El-Wastani gas field, onshore Nile Delta, Egypt. Arab. J. Geosci., 15, 1–29, 2022.

Farouk, S., Ziko, A., Eweda, S. A., and Said, A. E.: Subsurface Miocene sequence stratigraphic framework in the Nile Delta, Egypt. J. Afr. Earth Sci., 91, 89–109, 2014.

Fornaciari, E., Di Stefano, A., Rio, D., and Negri, A.: Middle Miocene quantitative calcareous nannofossil biostratigraphy in the Mediterranean region, Micropaleontology, 42, 37–63, 1996.

Gibbs, S. J., Shackleton, N. J., and Young, J. R.: Identification of dissolution patterns in nannofossil assemblages: A high-resolution comparison of synchronous records from Ceara Rise, ODP Leg 154, Paleoceanography, 19, PA1029, https://doi.org/10.1029/2003PA000958, 2004.

Haq, B. U., Hardenbol, J., and Vail, P. R.: Chronology of fluctuating sea levels since the Triassic, Science, 235, 1156–1167, 1987.

Hardenbol, J., Thierry, J., Farley, M. B., Jacquin, T., De Graciansky, P. C., and Vail, P. R.: Mesozoic and Cenozoic sequence chronostratigraphic framework of European basins, in: Sequence Stratigraphy of European Basins, edited by: de Graciansky, P.-C., Hardenbol, J., Jacquin, T., and Vail, P. R., SEPM Special Publication, 60, 3–14, 1998.

Harms, J. and Wray, J.: Nile Delta, in: Geology of Egypt, edited by: Said, R., A. A. Balkema/Rotterdam/Brookfield, John Wiley & Sons, 329–343, ISBN 978-9061918561, 1990.

Holbourn, A., Henderson, A. S., and Macleod, N.: Atlas of benthic foraminifera: first edition Wiley-Blackwell, Natural History Museum, John Wiley & Sons, 651 pp., ISBN 9781118389805, 2013.

Iaccarino, S.: Mediterranean Miocene and Pliocene planktic foraminifera, in: Plankton Stratigraphy, Bolli, H. M., Saunders, J. B., and Perch-Nielsen, K., Cambridge University Press, 283–314, https://doi.org/10.1017/S0016756800035214, 1985.

Iaccarino, S. and Salvatorini, G.: A framework of planktonic foraminiferal biostratigraphy for Early Miocene to Late Pliocene Mediterranean area, Paleontol. Stratigr. Evol., 2, 115–125, 1982.

Iaccarino, S. M., Premoli Silva, I., Biolzi, M., Foresi, L. M., Lirer, F., and Turco, E.: Practical manual of Neogene planktonic foraminifera, International School on Planktonic Foraminifera, (Neogene Planktonic Foraminifera), Università di Perugia Press, 1–180, 2007.

Ismail, A. A., Boukhary, M., and Abdel Naby, A. I.: Subsurface stratigraphy and micropaleontology of the Neogene rocks, Nile Delta, Egypt. Geol. Croat., 63, 1–26, 2010.

Kamel, H., Eita, T., and Sarhan, M.: Nile Delta hydrocarbon potentiality, Egypt, EGPC. 14th Petr. Explor. and Production Conf., Egyptian General Petroleum Corporation (EGPC), v.2, 485–503, ISBN 9781629810683, 1998.

Kassab, M. A., Teama, M. A., Cheadle, B. A., El-Din, E. S., Mohamed, I. F., and Mesbah, M. A.: Reservoir characterization of the Lower Abu Madi Formation using core analysis data: El-Wastani gas field, Egypt. J. Afr. Earth Sci., 110, 116–130, 2015.

Kellner, A., El Khawaga, H., Brink, G., Brink-Larsen, S., Hesham, M., El Saad, H. A., Atef, A., Young, H., and Finlayson, B.: Depositional history of the West Nile Delta–upper Oligocene to upper Pliocene: AAPG Memoir, Search Discovery Article 30092, American Association of Petroleum Geologists (AAPG), ISBN 978-0891813729, 2009.

Leckie, R. M. and Olson, H. C.: Foraminifera as proxies for sea-level change on siliciclastic margins, in: Micropaleontologic Proxies of Sea-Level Change and Stratigraphic Discontinuities, edited by: Olson, H. C. and Leckie, R. M., SEPM Spec. Publ., 75, 5–19, https://doi.org/10.2110/pec.03.75.0005, 2003.

Lirer, F., Foresi, L. M., Iaccarino, S. M., Salvatorini, G., Turco, E., Cosentino, C., Sierro, F. J., and Caruso, A.: Mediterranean Neogene planktonic foraminifer biozonation and biochronology, Earth. Sci. Rev., 196, 102869, https://doi.org/10.1016/j.earscirev, 2019.

Loeblich, A., and Tappan, H.: Foraminiferal Genera and their Classification, VNRC, New York, 970 pp., https://doi.org/10.1007/978-1-4899-5760-3, 1988.

Lourens, L. J., Hilgen, F. J., Shackleton, N. J., Laskar, J., and Wilson, D.: The Neogene period, in: Geological Time Scale 2004, edited by: Gradstein, F. M., Ogg, J. G., and Smith, A. G., Cambridge University Press, 409–440, https://doi.org/10.1017/CBO9780511536045, 2004.

Martini, E.: Standard Tertiary and Quaternary calcareous nannoplankton zonation, in: Proc. 2nd Int. Conf., edited by: Farinacci, A., Planktonic Microfossils Roma, Editura Tecnoscienza, Rome 2, 739–785, ISBN 3-900312-54-0, 1971.

Miller, K. G., Browning, J. V., Aubry, M.P., Wade, B. S., Katz, M. E., Kulpecz, A. A., and Wright, J. D.: Eocene–Oligocene global climate and sea-level changes: St. Stephens Quarry, Alabama, Geol. Soc. Am. Bull., 120, 34–53, 2008.

Monechi, S., Angori, E., and Von Salis, K.: Calcareous nannofossil turnover around the Paleocene/Eocene transition at Alamedilla (southern Spain), Bull. Soc. Geol. France, 171, 477–489, 2000.

Murray, J.: Ecology and palaeoecology of benthic foraminifera: Longman Scientific and Technical, Harlow, England, 397 pp., https://doi.org/10.1017/S0025315400053650, 1991.

Murray, J. W.: Ecology and applications of benthic foraminifera, Cambridge university press, Cambridge (UK), 426 pp., https://doi.org/10.1017/CBO9780511535529, 2006.

Nio, S. D., Brouwer, J., Smith, D., De Jong, M., and Böhm, A.: Spectral trend attribute analysis: applications in the stratigraphic analysis of wireline logs. first break, J. Pet. Geol. Spec. Topic, 23, 71–75, 2005.

Okada, H. and Bukry, D.: Supplementary modification and introduction of code numbers to the low-latitude coccolith biostratigraphy, Mar. Micropaleontol., 5, 321–325, 1980.

Ogg, J. G., Ogg, G. M., and Gradstein, F. M.: A concise geologic time scale, Elsevier, 187–201, ISBN 9780444637710, 2016.

Raffi, I., Mozzato, C., Fornaciari, E., Hilgen, F. J., and Rio, D.: Late Miocene calcareous nannofossil biostratigraphy and astrobiochronology for the Mediterranean region, Micropaleontology, 49, 1–26, 2003.

Rizzini, A., Vezzani, F., Cococcetta, V., and Milad, G. J.: Stratigraphy and sedimentation of a Neogene-Quaternary section in the Nile Delta area (ARE), 5th Explor. Semin., Cairo, Elsevier, 1–42, https://doi.org/10.1016/0025-3227(78)90038-5, 1976.

Rizzini, A., Vezzani, F., Cococcetta, V., and MILAD, G.: Stratigraphy and sedimentation of Neogene – Quaternary section in the Nile Delta Area (A.R.E.), 5th Expl. Seminar, Cairo, 1–42, 1976.

Rizzini, A., Vezzani, F., Cococcetta, V., and Milad, G. J.: Stratigraphy and sedimentation of a Neogene- Quaternary section in the Nile Delta area (ARE), Mar. Geol., 27, 327–348, 1978.

Roveri, M., Flecker, R., Krijgsman, W., Lofi, J., Lugli, S., Manzi, V., and Sierro, F.: The Messinian Salinity Crisis: past and future of a great challenge for marine sciences, Mar. Geol., 352, 25–58, 2014.

Said, R.: The geologic evolution of the River Nile, New York, Springer, 151 pp., https://doi.org/10.1007/978-1-4612-5841-4, 1981.

Selim, S. S., Abd El-Gwad, M. A., and Khadrah, A. A.: Sedimentology, petrography, hydraulic flow units, and reservoir quality of the bayhead delta reservoirs: Late Messinian Qawasim formation, Nile Delta, Egypt. Mar. Pet. Geol., 130, 105–125, 2021.

Selim, S. S., Abdel-Moaty, H. S., and Darwish, M.: Sedimentology and reservoir characteristics of delta plain reservoirs: An example from Messinian Abu Madi Formation, Nile Delta, Mar. Pet. Geol., 139, 105623, https://doi.org/10.1016/j.marpetgeo.2022.105623, 2022.

Selima, A.: Late Neogene stratigraphy and paleoecology in Wadi Wizr, Red Sea Coast, Egypt. Egypt. J. Geol., 42, 419–438, 1998.

Sestini, G.: Egypt, in: Regional Petroleum Geology of The World, Part II: Africa, America, Australia and Antarctica (Beiträge zur regionalen Geologie der Erde, edited by: Kulke, H., Gebrüder Borntraeger Verlagsbuchhandlung, Stuttgart, 22, 66–87, ISBN 9783443110222, 1995.

Sinaci, M.: Fluctuations of sea water temperature based on nannofloral changes during the Middle to Late Miocene, Adana Basin, Turkey, Turk. J. Earth Sci., 22, 247–263, 2013.

Snedden, J. and Liu, C.: A compilation of Phanerozoic sea-level change, coastal onlaps and recommended sequence designations: AAPG, Int. Conf. and Exhib., Search discovery article, 3, 40594, https://doi.org/10.1306/01031110138, 2010.

Sprovieri, R., Bonomo, S., Caruso, A., Di Stefano, A., Di Stefano, E., Foresi, L. M., Iaccarino, S. M., Lirer, F., Mazzei, R., and Salvatorini, G.: An integrated calcareous plankton biostratigraphic scheme and biochronology for the Mediterranean Middle Miocene, Riv. Ital. Paleontol. Stratigr., 108, 337–353, 2002.

Srinivasan, M. S. and Kennett J. P.: The oligocene-miocene boundary in the South Pacific, Geol. Soc. Am. Bull., 94, 798–812, 1983.

Van der Zwann, G. J., Jorissen, F. J., and de Stigter H. C.: The depth dependency of planktonic/benthic foraminiferal ratios: constraints and applications, Mar. Geol., 95, 1–16, 1990.

Van Morkhoven, F. P. C. M., Berggren, W. A., and Edwards, A. S.: Cenozoic cosmopolitan deep-water benthic foraminifera, Centers de Recherches Explor-Prod Elf-Aquitaine Mémoire, 11, p. 421, ISBN 9782901026204, 1986.

Verducci, M., Foresi, L. M., Scott, G. H., Sprovieri, M., Lirer, F., and Pelosi, N.: The Middle Miocene climatic transition in the Southern Ocean: evidence of paleoclimatic and hydrographic changes at Kerguelen plateau from planktonic foraminifers and stable isotopes, Palaeogeogr. Palaeocl., 280, 371–386, 2009.

Villa, G., Fioroni, C., Pea, L., Bohaty, S., and Persico, D. J.: Middle Eocene – late Oligocene climate variability: calcareous nannofossil response at Kerguelen Plateau, Site, 748, 173–192, 2008.

Wade, B. S. and Bown, P. R.: Calcareous nannofossils in extreme environments: the Messinian salinity crisis, Polemi Basin, Cyprus, Palaeogeogr. Palaeocl., 233, 271–286, 2006.

Wade, B. S., Pearson, P. N., Berggren, W. A., and Pälike, H.: Review and revision of Cenozoic tropical planktonic foraminiferal biostratigraphy and calibration to the geomagnetic polarity and astronomical time scale, Earth Sci. Rev., 104, 111–142, 2011.

Wei, W., Villa, G., and Wise, S. W.: Paleoceanographic implications of EoceneOligocene calcareous nannofossils from Sites 711 and 748 in the Indian Ocean. Proceedings of the Ocean Drilling Program, Sci. Res., 120, 979–999, 1992.

Wei, W. and Wise, S. W.: Biogeographic gradients of middle Eocene-Oligocene calcareous nannoplankton in the South Atlantic Ocean, Palaeogeogr. Palaeocl., 79, 29–61, 1990.

Wornardt, W.: Revision of sequences boundaries and maximum flooding surfaces: Jurassic to Recent, Offshore Technology Conference (OTC) , Houston, Texas, 3–6 May, OnePetro, https://doi.org/10.4043/14072-MS, 1999.